Cell Calcium 78 (2019) 1–14

Contents lists available at ScienceDirect

Cell Calcium

journal homepage: www.elsevier.com/locate/ceca

# Regulation of $Ca^{2+}$ signaling by acute hypoxia and acidosis in cardiomyocytes derived from human induced pluripotent stem cells

José-Carlos Fernández-Morales[a], Wei Hua[a], Yuyu Yao[a], Martin Morad[a,b,*]

[a] Cardiac Signaling Center of MUSC, USC and Clemson, Charleston, SC, USA
[b] Department of Pharmacology,Georgetown University Medical Center, Washington, DC, USA

ARTICLE INFO

*Keywords:*
L-type Ca(2+) channel
Hypoxia
Acidosis
Ischemia
Human induced pluripotent stem cells derived cardiomyocytes

ABSTRACT

*Aims:* The effects of acute (100 s) hypoxia and/or acidosis on $Ca^{2+}$ signaling parameters of human induced pluripotent stem cell-derived cardiomyocytes (hiPSC-CM) are explored here for the first time.
*Methods and results:* **1)** hiPSC-CMs express two cell populations: *rapidly-inactivating* $I_{Ca}$ myocytes ($\tau_i < 40$ ms, in 4–5 day cultures) and *slowly-inactivating* $I_{Ca}$ ($\tau_i \geq 40$ ms, in 6–8 day cultures). **2)** Hypoxia suppressed $I_{Ca}$ by 10–20% in rapidly- and 40–55% in slowly-inactivating $I_{Ca}$ cells. **3)** Isoproterenol enhanced $I_{Ca}$ in hiPSC-CMs, but either enhanced or did not alter the hypoxic suppression. **4)** Hypoxia had no differential suppressive effects in the two cell-types when $Ba^{2+}$ was the charge carrier through the calcium channels, implicating $Ca^{2+}$-dependent inactivation in $O_2$ sensing. **5)** Acidosis suppressed $I_{Ca}$ by ~35% and ~25% in rapidly and slowly inactivating $I_{Ca}$ cells, respectively. **6)** Hypoxia and acidosis suppressive effects on Ca-transients depended on whether global or RyR2-microdomain were measured: with acidosis suppression was ~25% in global and ~37% in RyR2 $Ca^{2+}$-microdomains in either cell type, whereas with hypoxia suppression was ~20% and ~25% respectively in global and RyR2-microdomaine in rapidly and ~35% and ~45% respectively in global and RyR2-microdomaine in slowly-inactivating cells.
*Conclusions:* Variability in $I_{Ca}$ inactivation kinetics rather than cellular ancestry seems to underlie the action potential morphology differences generally attributed to mixed atrial and ventricular cell populations in hiPSC-CMs cultures. The differential hypoxic regulation of $Ca^{2+}$-signaling in the two-cell types arises from differential $Ca^{2+}$-dependent inactivation of the $Ca^{2+}$-channel caused by proximity of $Ca^{2+}$-release stores to the $Ca^{2+}$ channels.

## 1. Introduction

Ischemic heart disease and acute myocardial infarction are leading causes of death from cardiovascular pathology in developing countries [1]. Myocardial infarction often triggers arrhythmia when the human heart is subjected to acute hypoxia during coronary occlusion or when oxygen demands of the heart exceeds its work load [2]. The development of cardiomyocytes derived from human induced pluripotent stem cells (hiPSC-CMs), not only is a promising strategy for patient-specific cell therapy [3,4], but also allows *in vitro* experimental approach to study the mechanisms underlying cardiac pathology in human tissue [5]. Recent reports suggest that hiPSC-CMs are a good *in vitro* electrophysiological model of human cardiomyocytes because: 1) similar to mature mammalian cardiomyocytes, hiPSC-CMs express robust levels of L-type $Ca^{2+}$ channels and $Ca^{2+}$-induced $Ca^{2+}$ release (CICR), critical for EC-coupling [6–9]; 2) regulation of the L-type $Ca^{2+}$ channels and calcium signaling by $Ca^{2+}$, phosphorylation, and pharmacological agents in hiPSC-CMs mimics closely that of mammalian cardiomyocytes [10,11]. Encouraged by possible human-relevance of these reports, we probed the pathophysiological effects of hypoxia and ischemia in hiPSC-CMs [12]. Although there are a few reports on the effects of chronic hypoxia in hiPSC-CMs [13–16], there are no reports on the effects of acute hypoxia and acidosis on calcium signaling of hiPSC-CMs. Since L-type cardiac $Ca^{2+}$ channels have been implicated in oxygen-sensing of the rat heart [17] through a mechanism involving the interaction of heme-oxygenase with CaM/CaMKII domain of L-type $Ca^{2+}$ channel [18], it was critical to determine whether similar mechanism are also at play in human stem cell-derived cardiomyocytes

*Abbreviations:* APs, action potentials; $[Ca^{2+}]_i$, intracellular calcium-concentration; CDI, calcium-dependent inactivation; CICR, calcium-induced calcium release; FKBP-GCaMP6, RyR2-targeted $Ca^{2+}$ biosensor; hiPSC-CMs, human induced pluripotent stem cell-derived cardiomyocytes; $I_{Ca}$, calcium current; ISO, Isoproterenol; ROS, reactive oxygen species; rN-CMs, rat neonatal ventricular cardiomyocytes; RYR, ryanodine receptor; SR, sarcoplasmic reticulum

* Corresponding author at: Cardiac Signaling Center, USC, MUSC & Clemson University, Charleston, SC, 29425, USA.
*E-mail address:* moradm@musc.edu (M. Morad).

https://doi.org/10.1016/j.ceca.2018.12.006
Received 9 September 2018; Received in revised form 11 December 2018; Accepted 11 December 2018
Available online 12 December 2018

thus obviating possible subtle species differences in the hypoxic responses and its adrenergic regulation between adult and neonatal rat cardiomyocytes [19] and human heart.

Here we explored the effects of acute hypoxia and acidosis on human iPS-derived cardiomyocytes and found that the susceptibility to hypoxia and acidosis was partly dependent on the inactivation kinetics of L-type $Ca^{2+}$ channels. Generally, two groups of cells were consistently identified: those with rapidly inactivating $I_{Ca}$, time constant ~ 10 ms and those with slowly inactivating $I_{Ca}$, tau ~40 ms. Our data suggests that the older slowly inactivating $I_{Ca}$ cells were more sensitive to hypoxia but not to acidosis as compared to younger rapidly inactivating $I_{Ca}$ cells.

## 2. Methods

### 2.1. Cell culture of human pluripotent stem cells and cardiac differentiation

Human pluripotent stem cells (hiPSC-K3) obtained from Stephen Duncan at Medical University of South Carolina [20] were routinely cultured in E8 medium (Life Technologies/GIBCO) on Matrigel (BD Biosciences) coated tissue culture plates with daily media change at 37 °C with 5% (vol/vol) $CO_2$. Differentiation was performed following the protocols of Xiaojun Lian et al [21]. Briefly, dissociated hiPSCs were plated in 12 well plates with matrigel and then treated with 12 μM CHIR 99021, a GSK3β inhibitor for 24 h in RPMI/B-27 without insulin. 72 h after CHIR99021 treatment, 5 mM IWP2, a *wnt* processing inhibitor, was added to culture with the same media for 48 h. After 48 h of continued culture in RPMI/B-27 without insulin, the cells were maintained in RPMI/B-27 medium with insulin for the rest of the time.

### 2.2. hiPSC-CMs dissociation

The hiPSC-CM cell lines were grown in culture for 30–40 days before dissociating and re-plating for electrophysiological and $Ca^{2+}$ imaging experiments. The mechanical dissociation of hiPSC-CM clusters into single cardiomyocytes has been made following the next protocol: 1) Visualize spontaneously beating EBs under the microscope, and mechanically dissect them from the gelatin coated wells with a curved 23 G needle. 2) Aspirate the dissected EBs with their original medium using pipette and transfer them to a 50 ml test tube. 3) Centrifuge the EBs suspension within the test tube at a rate of 1000 rpm for 5 min. 4) Re-suspend the EBs in 10 ml of fresh medium and transfer them to a 15 ml test tube. 5) Centrifuge at a rate of 900 rpm for 2 min. 6) Wash the cells 3 × with PBS (centrifuge between washings at a rate of 900 rpm for 2 min). 7) Add 5 ml of 1 mg/ml collagenase type IV solution (5 mg collagenase IV-low $Ca^{2+}$ solution) to the centrifuged washed cells. 8.) Incubate the solution with EBs in 37 °C bath for 5 min. 9) Incubate with rotator for additional 45 min in 37 °C. 10) Centrifuge at a rate of 1000 rpm for 5 min. 11) Re-suspend cells with 3 ml of re-suspension solution. Incubate in 37 °C for additional 15 min. 12) Centrifuge at a rate of 1000 rpm for 5 min. The single hiPSC-CMs then were plated on fibronectin (2.5 μg/ml)-coated glass coverslips in 6 well plates after collagenase B treatment, and then incubated for 36–72 h before their use in electrophysiological or $Ca^{2+}$ imaging experiments.

### 2.3. Electrophysiological recordings

Whole-cell $Ca^{2+}$ currents ($I_{Ca}$) was recorded using the perforated-patch mode of the patch-clamp technique [22,23], induced by amphotericin B (1 mg/ml) [24,25]. After waiting approximately 5–10 min, series resistance fell below 20 MΩ and tight seals (> 1 GΩ) were achieved using an intracellular solution composed (in mM): 145 Glutamic Acid, 9 NaCl, 1 $MgCl_2$ and 10 HEPES, pH 7.2 ~ 7.3, adjust with CsOH. Cells were bathed in a Tyrode's solution composed of (in mM): 137 NaCl, 1 $MgCl_2$, 2 $CaCl_2$ or 2 $BaCl_2$ (depending on the experimental protocol), 5.3 KCl, 10 glucose, and 10 HEPES. The duration of different experimental treatments (Normoxia/Hypoxia and/or pH 7.4/pH 6.7, with or without ISO in all the figures of the manuscript was always 100 s, except for the washing of ISO in normoxia condition, lasting often ~ 200 s. In all experiments $I_{Ca}$ was recorded at room temperature (22–25 °C) using a Dagan voltage-clamp amplifier controlled by pClamp-9 software running on a personal computer. Borosilicate patch pipettes with 5–7 MΩ resistance were prepared the previous hour using a horizontal pipette puller (Model P-87, Sutter Instruments, CA). The series resistance was monitored until it decreased to < 20 MΩ, after which the experiments were began. The liquid junction potential was corrected before seal formation. In all recordings, the holding potential was set at −40 mV in order to inactivate $Na^+$ channels. $I_{Ca}$ or $I_{Ba}$ were activated by100-ms depolarizing voltage pulses to 0 mV. $I_{Ca}$ or $I_{Ba}$ were measured at 5 s intervals except when electrophysiological measurements were combined with fluorescence measurements, in which case they were measured 25 s intervals. The measured currents were filtered at 1 or 10 kHz, digitized at 10 or 100 kHz, and plotted and analyzed in terms of magnitude and time constants of their inactivation, using Graph Prism (GraphPad Corp., San Diego, CA, USA) and pCLAMP 9.0 software. Membrane potential (Em) oscillations were registered using the current-clamp configuration of the patch-clamp technique. The holding potential was set at -50 mV in voltage clamp mode, and the series resistance continuously monitored until it had decreased to < 20 MΩ. After this the amplifier was shifted to the current-clamp mode, (with no current "injection" applied). Only cells with leak currents of < 5 pA were used for experimental analysis. Cell size was estimated from membrane capacitance measurements, a method commonly utilized to obtain an estimate of the plasma membrane area of the cells, providing an indirect indicator of the cell size. This approach is particularly useful in hiPSC-CMs which have few membrane invaginations or t-tubular system at these stages of development [26,27]. Note that earlier studies have shown a positive linear correlations between membrane capacitance and cell volume in cardiomyocytes of several species [28].

To study the effects of hypoxia on ionic currents, single voltage-clamped hiPSC-CMs were perfused with external Tyrode's solutions equilibrated with atmospheric $O_2$ (normoxic) or 100% $N_2$ (hypoxic). We bubbled hypoxic solutions for at least 1 h to make sure that nitrogen displaces all the oxygen molecules from our reservoirs and then we began the rapid application of the hypoxia solution by the perfusion pipette placed in close proximity of the cell. Solution exchange took place within 50 ms using an electronically controlled perfusion system equipped with five barrels loaded with normoxic and hypoxic Tyrode's solutions containing varying electrolyte concentrations and pharmacological agents desired for the different type of experiments [29]. The $O_2$ pressure was measured with a needle probe which registered < 5 mmHg for the hypoxic solutions both in the bubbled reservoirs and near the port for solution outflow into the main chamber. HEPES (10 mM) was used to buffer the extracellular solutions, which prevented changes in the pH of the external solutions with bubbling of $N_2$. Acidification of the media to pH 6.7 was achieved by addition of isotonic HCl. The pH of all solutions was carefully determined using a pH meter at room temperature (~ 25 °C).

### 2.4. Fluorometric $Ca^{2+}$ measurements in voltage-clamped cells

Single isolated beating hiPSC-CMs were subjected to 100 ms depolarizing voltage-clamp pulses (-40 to 0 mV) that activated $I_{Ca}$ triggering intracellular $Ca^{2+}$ transients. Intracellular global $Ca^{2+}$ signals were measured with the fluorescent $Ca^{2+}$- indicator dye Fluo-4 AM (2 μM, Invitrogen), after 40 min of incubation of cells at 37 °C and 5% $CO_2$. The fluorescence probe and dye were excited at 460 nm using a LED-based illuminator (Prismatix, Modiin Ilite, Israel) and gated aperture and $Ca^{2+}$-dependent fluorescent light (> 500 nm) was detected with a photomultiplier tube using a Zeiss Axiovert 100 TV inverted microscope.

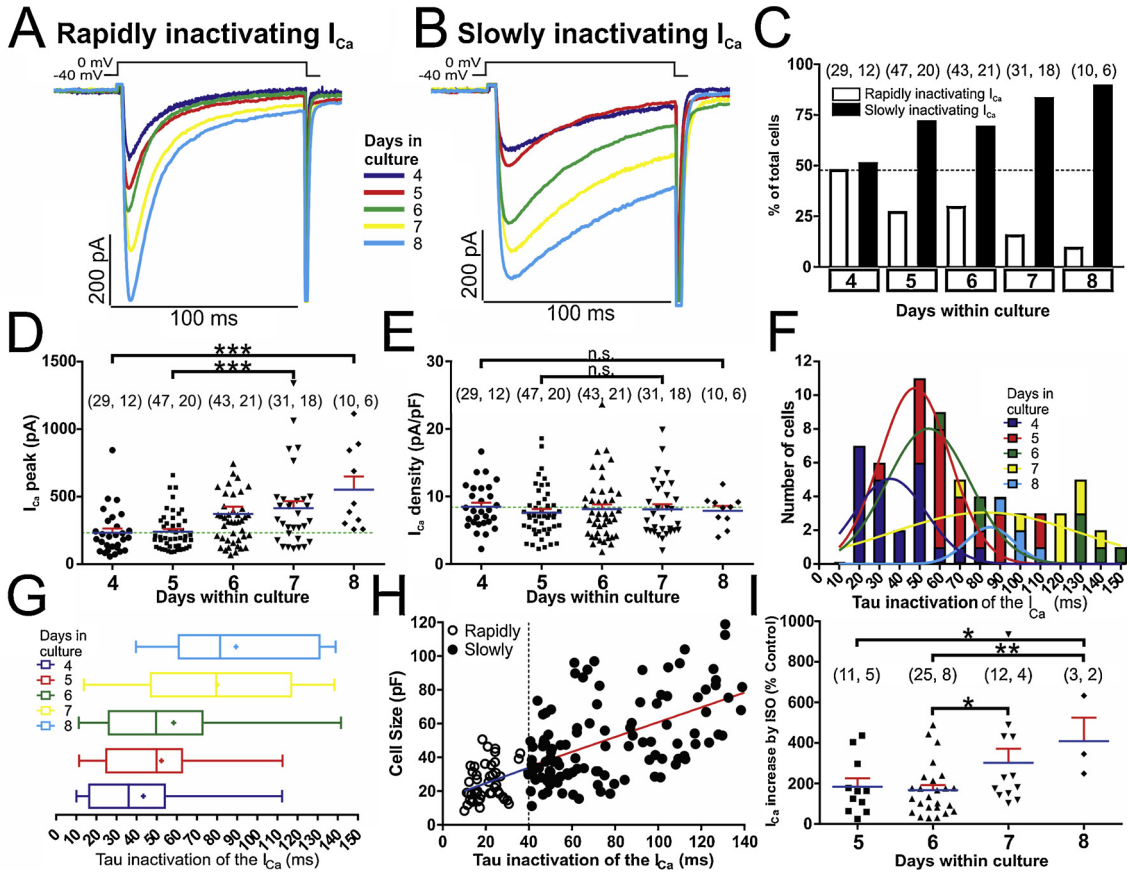


**Fig. 1.** Two different time dependent kinetics of L-type calcium channels are expressed in cultured hiPSC-CMs. Panels A and B show examples of original traces of calcium currents obtained from different hiPSC-CMs with variable ages in culture (4–8 days), activated by depolarization from -40 mV to 0 mV, exhibiting different rates of inactivation: Rapidly inactivating $I_{Ca}$ (Panel A) and slowly inactivating $I_{Ca}$ (Panel B). Panel C shows a plot of the cell percentages that presented rapidly or slowly inactivating $I_{Ca}$ vs. the age of the cells in culture. Panel D and E, presented as dot plots, represent the individual cell values of $I_{Ca}$ and $Ca^{2+}$ current density respectively vs. cell time in culture (4–8 days); the mean is represented by blue bars and the standard error of the mean by the red error bars. Panel F and G provide frequency histograms and box and whiskers plots respectively showing the distribution of the inactivation time constant of the $I_{Ca}$ ($\tau_i$) at the five different time in culture (4, 5, 6, 7 and 8 days). The data were pooled in such a way that the number of observations with 0.00 ms $\leq \tau_i <$ 10.00 ms were plotted in the column $\tau_i$ = 10 ms and in the same way with the rest of observations. The data were fitted to a Normal Distribution with five different colors Gauss curve represented (dark blue, red, green, yellow and light blue for hiPSC-CMs with 4, 5, 6, 7 or 8 days in culture respectively). Data distribution are presented also in box-and-whiskers plots with the same colors/days in culture scheme: the line inside the box depicts median values, the size of the box is given by the distance between the 25th and the 75th percentiles; right "whisker" reach the 90th percentile and left "whisker" the percentile 10th. Means are also represented inside the box with a cross symbol. Panel H shows a scatter-graph plot of cell size (pF) vs. inactivation time constant ($\tau_i$) from hiPSC-CMs with rapidly (○) and slowly (●) inactivating $I_{Ca}$, hiPSC-CMs were classified as expressing rapidly- ($\tau_i \leq$ 40 ms) or slowly-inactivating ($\tau_i >$ 40 ms) L-type $Ca^{2+}$ channels. Panel I is represented as a dot plot, showing the distribution of individual cell values of $I_{Ca}$ increased (in % with respect to the $I_{Ca}$ peak under control conditions without ISO) during the treatment with 100 nM isoproterenol at the time of the cells in culture (5–8 days). In panels C, D, E and I, for each of the different data groups, the number of cells ($n$) and the number of different cultures conducted to obtain these data (N) are indicated in parentheses as ($n$, N). Data were presented as the mean ± SEM in this figure. We used one-way ANOVA with post-hoc multiple comparisons using the Tukey's multiple comparisons test for unpaired parametric comparisons. *$P <$ 0.05; **$P <$ 0.01; n.s.: not significant. (For interpretation of the references to colour in this figure legend, the reader is referred to the web version of this article).

Focal RyR2 $Ca^{2+}$ micro-domains were measured using genetically engineered virally introduced biosensors GCaMP6-FKBP targeted to FKBP-12.6 (calstabin-2) binding site of RyR2 ($K_d$ = 250 nM, $\lambda_{ex}$ = 488 nm). The probe uses calmodulin as $Ca^{2+}$ chelator and green fluorescent protein (GFP) as reporting fluorophor, which allows it to sense the $Ca^{2+}$ in the micro-domains of dyadic clefts where CICR takes place. For the probe and the fluorescent $Ca^{2+}$- indicator dye the parameters of the $Ca^{2+}$ signals analyzed were the basal fluorescence ($F_0$) and the peak of the $Ca^{2+}$ transient (ΔF).

### 2.5. Chemical products

Chemical compounds to make saline solutions, as well as isoprenaline hydrochloride were purchased from Sigma (Sigma-Aldrich, St Louise, MO, USA). Amphotericin B was acquired from Fisher Scientific (Pittsburgh, PA, USA). Every experimental day, a stock solution of isoprenaline hydrochloride was prepared in deionized water and amphotericin B in DMSO. The inhibitors CHIR 99021 were acquired from Selleckchem (Houston, TX, USA) and IWP2 from TOCRIS (Minneapolis, MN, USA), E8, RPMI and B-27 culture mediums were purchased from Life Technologies/GIBCO (Grand Island, NY, USA). The novel and potent $Ca_V$1.3-highly selective antagonist, 1-(3-chlorophenethyl)-3-cyclopentylpyrimidine-2,4,6-(1*H*,3*H*,5*H*)-trione [30], was purchased from Calbiochem-EMD chemicals (San Diego, CA, USA).

### 2.6. Statistical analysis

Data are presented as scatter grams, showing the individual data points of each cell together with the mean (represented in blue line) ± standard error of the mean (SEM, represented by the red error lines). The number of cells and cultures are indicated in parentheses ($n$, $N$). Paired or unpaired two-tailed Student's $t$ test was used to compare

means according to the dependent or independent between the data set to compare. A $P$ value equal or smaller than 0.05 was selected as the limit of significance. Significance levels were indicated with an increasing number of asterisks ($*P < 0.05$, $**P < 0.01$, $***P < 0.001$) and when not being significant by (n.s., $P > 0.05$). Data sets were tested for normality (Kolmogorov-Smirnov normality test), an assumption for the application of the Student's *t*-test. We found that some groups didn't fit well to normal distributions, a nonparametric statistical test was used (Mann-Whitney's rank sum test to compare two samples). In other cases, one-way ANOVA with post-hoc multiple comparisons was used to establish if there were significant differences between the means of 3 or more independent groups, not related to each other. Scatter plot were used to explore the association between cell size, the suppression of the $I_{Ca}$ by hypoxia and the tau inactivation of the $I_{Ca}$. The correlations between these variables were analyzed by Pearson linear correlation coefficient. To analyze $I_{Ca}$ decay or *tau inactivation* of the $I_{Ca}$ ($\tau_i$), single exponential fits were applied to the decaying part of individual $I_{Ca}$ traces using a simplex optimization algorithm as follows: $y = y_0 + \{1 - [A_i \exp(- t / \tau_i)]\}$ where $A_i$ represent the amplitudes of the $I_{Ca}$ and $\tau_i$ represent the time constants of inactivation respectively. To study the tail currents triggered by calcium channel deactivation, the tail current time course of rapidly and slowly inactivating $I_{Ca}$ cells were fitted by a bi-exponential equation with a fast ($\tau_1$) and slow ($\tau_2$) time constants. The bi-exponential fitting produces similar correlation coefficient average that using mono-exponential fitting (0.968 vs. 0.988) and precision ($1e^{-4}$ for both cases). We also analyzed the peak amplitude of the $I_{Ca}$ tail for both cell types. All statistical analysis was performed using GraphPad Prism 7.0 (GraphPad Software, La Jolla, CA) and MS Excel (Microsoft, Redmond, WA).

## 3. Results

### 3.1. Two different cell populations of hiPSC-CMs cultures based on $Ca^{2+}$ channel inactivation kinetics

#### 3.1.1. Pharmacological, biophysical and molecular characterization

Calcium currents were measured in hiPSC-CMs in 4 to 8 day cultures using the perforated-patch mode of the whole-cell patch-clamp technique, (day zero was the day of the mechanical dissociation of hiPSC-CM clusters into single cardiomyocytes). Unexpectedly, we found two distinct populations of hiPSC-CMs based on the inactivation kinetics of their $I_{Ca}$ (Fig. 1A and B). In one group of cells, $I_{Ca}$ inactivated rapidly ($\tau_i = 21.40 \pm 1.16$ ms, n = 48 cells), while in another set $I_{Ca}$ inactivated slowly ($\tau_i = 51.95 \pm 1.01$ ms, n = 56 cells). The latter group of cells were more abundant in older 6 to 8 day cultures (Fig. 1C, F). These two cell types were found on each single day in culture, but the percentage of cells with slowly inactivating $I_{Ca}$ was higher in older cultures while those with rapidly inactivating $I_{Ca}$ decreased from 48.3% at day 4 to 10.0% at day 8 of culture, Fig. 1C. A positive linear correlation (r = 0.548 p < 0.0001) was found between the cell surface area (pF) and the inactivation time constant of $I_{Ca}$ ($\tau_i$), Fig. 1H. Smaller cells (10–30 pF) had mainly rapidly inactivating $I_{Ca}$, while cells larger than 30 pF had escalating slower inactivation kinetics. The dashed vertical line at $\tau_i = 40$ ms was arbitrarily set as separation of the two cell populations (open circles, $\tau_i < 40$ ms, and those with much slower inactivating $I_{Ca}$, filled circles, $\tau_i \geq 40$ ms).

The distribution of the inactivation time constant ($\tau_i$) of $I_{Ca}$ in different days of culture could be differentiated into three main groups, based on the center of bell-shaped distributions: first group, at 4 days' culture centered at ~35 ms, second group, centered at ~55 ms at 5 and 6 days, and the third group, centered at ~85 ms at 7 and 8 days of culture (Fig. 1F). Box and colored whiskers plots (dark blue, red, green, yellow and light blue) show the distribution of the $\tau_i$ for the 4, 5, 6, 7 days of culture, with median values of 36, 50, 50, 80 and 81 ms, respectively (Fig. 1G).

#### 3.1.2. Biophysical analysis

We explored the possibility of whether the calcium channels expressed in the two cell types producing $I_{Ca}$ with rapidly or slowly inactivating kinetics represent two different calcium channels (e.g. $Ca_V1.2$ and $Ca_V1.3$) or whether the same population of channels ($Ca_V1.2$) with different modulation of their CDI is responsible for the differences in the kinetics of inactivation of the two cell types. The analysis of kinetics of tail currents generated by deactivation of $I_{Ca}$ from 0 to -40 mVs in 60 cells fitted with two bi-exponential equation with a fast ($\tau_1$) and slow ($\tau_2$) time constants, Fig. S1, shows that the mean fast ($\tau_1$) and slow ($\tau_2$) time constants for the deactivation of the $I_{Ca}$ tail were not significantly different in the two cell types (Fig. S1 C and inset traces a2 & b2), consistent with the same population of channels being responsible for the two cell types.

#### 3.1.3. Molecular experiments

In support of single population idea, we found that the level of expression of $Ca_V1.2$ mRNA was markedly greater than $Ca_V1.3$ both in the early (day4) or late (day7) developmental time in culture where hiPSC-CMs with rapidly or slowly inactivating $I_{Ca}$, respectively, are more frequently found (Fig. S2). Consistent with mRNA studies 10 μM of a potent and selective $Ca_V1.3$ antagonist (1-(3-chlorophenethyl)-3-cyclopentylpyrimidine-2,4,6-(1*H*,3*H*,5*H*)-trione) [30], failed to block $I_{Ca}$ in hiPSC-CMs, where 2 or 10 μM nifedipine produced ~95% block of $I_{Ca}$ (panel D, Fig. 2).

***Pharmacologically*** also, the data suggests that one population of channels is responsible for the two different inactivation kinetics, because we found similar nifedipine sensitivity even in the presence of low concentrations of this dihydropyridine [31] and the same dose response relation for the rapidly and slowly inactivating $I_{Ca}$ (Fig. 2). These finding, therefore, suggest that only $Ca_V1.2$ subtype of L-type calcium channel is expressed in hiPSC-CMs but its CDI is differentially modulated during cell growth and development.

***Cell size***, estimated from membrane capacitance measurements increased significantly with culture age, reflecting cell growth, ranging from 27.50 ± 3.19 pF at day 4, to 31.61 ± 2.01 pF at day 5, to 45.69 ± 3.22 pF at day 6, to 50.97 ± 4.73 pF at day 7 and 69.98 ± 9.29 pF at day 8. Similarly, the $Ca^{2+}$ channel current increased significantly, from 233.51 ± 30.84 pA at day 4, to 240.59 ± 20.16 pA at day 5, to 371.94 ± 53.11 pA at day 6, to 413.87 ± 52.42 pA at day 7 and finally to 552.24 ± 97.52 pA at day 8 (Fig. 1A, B, D). However, $Ca^{2+}$ current density did not change significantly with the length of hiPSC-CMs in culture (8.49 ± 0.60 pA/pF at day 4, 7.61 ± 0.54 pA/pF at day 5, 8.14 ± 0.69 pA/pF at day 6, 8.12 ± 0.75 pA/pF at day 7 and 7.89 ± 0.73 pA/pF at day 8, Fig. 1E), suggesting that a gradual increase in the number of calcium channels occurred with the cell growth. Fig. 1I shows the differential potentiating effects of 100 nM isoproterenol (ISO) on $I_{Ca}$ as a function of days in culture, ~85% enhancement of $I_{Ca}$ at day 7 as compared to day 6, and almost ~150% enhancement at day 8 with respect to day 5 or 6.

***Action potential measurements*** in hiPSC-CMs cultures also reflected the decay kinetics of $I_{Ca}$, that is, cells with shorter action potentials expressed rapidly inactivating $I_{Ca}$ (Fig. 3B, C, H), and interestingly had a faster spontaneous pacing rate (Fig. 3A, I), while cells with longer action potential expressed slowly inactivating $I_{Ca}$ (Fig. 3E, F, H), and had much slower spontaneous pacing rates (Fig. 3D, I). Fig. 2G shows a positive linear correlation (r = 0.75 p < 0.0005) between the $APD_{90}$ (ms) and the inactivation time constant of $I_{Ca}$ ($\tau_i$), rapidly inactivating $I_{Ca}$ cells ($\tau_i \sim 20$ ms) had mainly shorter APs ($APD_{90} < 800$ ms) at room temperatures, while slowly inactivating $I_{Ca}$ cells ($\tau_i \geq 40$ ms) displayed progressively longer APs ($APD_{90} \geq 800$ ms). The dashed vertical line at $\tau_i = 40$ ms was chosen to denotes approximate separation of the two cell populations (squares, $\tau_i < 40$ ms, and those with much slower inactivating $I_{Ca}$, triangles, $\tau_i \geq 40$ ms). Spontaneously developing APs from rapidly inactivating $I_{Ca}$ cells also showed a significantly slower upstroke velocity (Fig. 3J). The resting membrane potential of the two

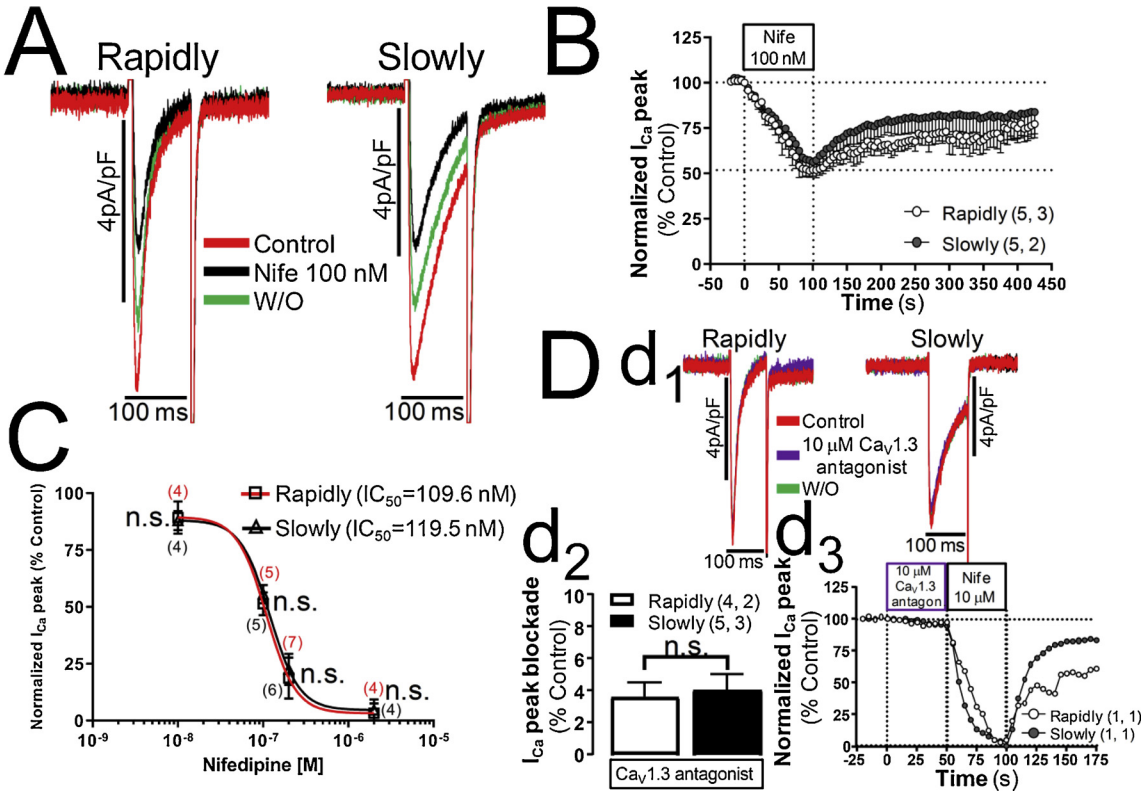


**Fig. 2.** Concentration-dependent blockade of the whole-cell $Ca^{2+}$ current elicited by nifedipine and a novel $Ca_V1.3$ antagonist in hiPSC-CMs with different inactivation kinetics. $I_{Ca}$ was recorded under the perforated-patch mode of the patch-clamp technique using 2 mM $Ca^{2+}$ as charge carrier and calcium currents were elicited by 100 ms depolarization pulses from -40 mV to 0 mV. Panel A show $I_{Ca}$ traces reduced after being perfused during 100 s with 100 nM nifedipine from hiPSC-CMs with rapidly and slowly inactivating $I_{Ca}$. Panel B show the time course of the $I_{Ca}$ blockade elicited by 100 nM nifedipine. In panel C are exposed the concentration-dependent blockade of the whole-cell $I_{Ca}$ peak elicited by nifedipine in hiPSC-CMs with rapidly and slowly inactivating $I_{Ca}$ with its corresponding values of $IC_{50}$, the sigmoidal concentration-response curves and the number of cells for each of the concentrations of nifedipine (10 nM, 100 nM, 200 nM and 2 μM) are shown in parentheses for rapidly inactivating $I_{Ca}$ cells (red color) and slowly inactivating $I_{Ca}$ cells (black). Panel D show the inapparent effect suppressing $I_{Ca}$ of a novel and selective $Ca_V1.3$ antagonist (1-(3-chlorophenethyl)-3-cyclopentylpyrimidine-2,4,6-(1*H*,3*H*,5*H*)-trione), in the subpanels inserted labeled as $d_1$ are represented $I_{Ca}$ traces at control level (red traces), 10 μM $Ca_V1.3$ antagonist (purple traces) and normoxia wash out (green traces) belonging to one of the hiPSC-CMs with rapidly inactivating $I_{Ca}$ and another with slowly inactivating $I_{Ca}$. The subpanel inserted labeled as $d_2$ plotted the average blocking effect on $I_{Ca}$ by 10 μM of the $Ca_V1.3$ antagonist in both cell types. Inserted subpanel $d_3$ show the time course of the blockade effect of $I_{Ca}$ elicited initially by the $Ca_V1.3$ antagonist and then by nifedipine 10 μM from two single cells with rapidly and slowly inactivation kinetics. The number of cells (*n*) and the number of different cultures (N) are indicated as (*n*, N). Data are mean ± SEM. n.s.: not significant; by paired Student's t-test (For interpretation of the references to colour in this figure legend, the reader is referred to the web version of this article).

cell types (data not shown) was not significantly different (~ −52 mV).

### 3.2. Hypoxia effects on cardiomyocytes derived from human induced pluripotent stem cells

#### 3.2.1. Suppressive effect of hypoxia on $I_{Ca}$ depends on its inactivation kinetics

Acute hypoxia was created by reducing $PO_2$ rapidly (< 1 s), exchanging the normoxic solution (equilibrated with ambient air, ~21% $O_2$) for a hypoxic solution (bubbled with 100% $N_2$; $PO_2$ < 5 mmHg). $I_{Ca}$ was activated with repeated depolarizations at 5 s intervals from −40 to 0 mV, to avoid possible activation of T-type $Ca^{2+}$ channels. Rundown was minimized by using perforated-patch mode of the patch-clamp technique, causing little or no significant decline in $I_{Ca}$ for periods of 3 min in normoxic solutions (Fig. 4C and D, empty circles). Rapid application of hypoxic solutions produced ~5% initial reduction of $I_{Ca}$ within the first 5 s in both cell types, continued by a gradual decrease in $I_{Ca}$ that stabilized within the first 60 s at 16.7 ± 2.6% (n = 8, N = 4) in cells with rapidly inactivating $I_{Ca}$ (Fig. 4C, filled circles). In slowly inactivating $I_{Ca}$ cells the suppression continued to increase reaching steady-state levels of 52.30 ± 9.4% (n = 8, N = 3) in ~100 s (Fig. 4D, filled circles). In both cell types $I_{Ca}$ recovered to its control levels in about 75 s following the return of normoxic solutions (Fig. 4C and D filled circles, see also original tracing of $I_{Ca}$ in two representative myocytes, Fig. 4A and B).

A positive linear correlation (r = 0.566, p < 0.001) was found between the degree of hypoxic suppression of $I_{Ca}$ and the rate of its inactivation (scatter-gram and red correlation line, Fig. 4E). Despite the great variability in the hypoxic suppressive effect, the slowly inactivating population of hiPSC-CMs (the predominant cell types, Fig. 1) were highly sensitive to hypoxia (~ 50% suppression), while hiPSC-CMs with rapidly inactivating $I_{Ca}$ were mostly resistant (~ 15% suppression) to acute hypoxia. Acute hypoxia also marginally, but not significantly, slowed the mean $I_{Ca}$ inactivation time constant from the normoxic values of 16.73 ± 3.85 ms and 43.21 ± 10.29 ms, Fig. 4F.

#### 3.2.2. Hypoxia effects on $Ba^{2+}$ transporting calcium channels

The suppressive effect of acute hypoxia was enhanced from 18% to 35% in adult rat cardiomyocytes when $Ba^{2+}$ was charge carrier through the channel [17,18]. Similarly, in rat neonatal cardiomyocytes suppression of CDI by $Ba^{2+}$ or by increased intracellular $Ca^{2+}$ buffering strongly enhanced the suppressive effects of hypoxia in the rapidly inactivating $I_{Ca}$ cells [19]. Fig. 5B shows that in hiPSC-CMs too, when 2 mM $Ba^{2+}$ replaced $Ca^{2+}$, acute hypoxia rapidly suppressed the current within the first 5 s, but in the slowly inactivating $I_{Ca}$ cells the steady-state suppression after 100 s of hypoxia was significantly smaller

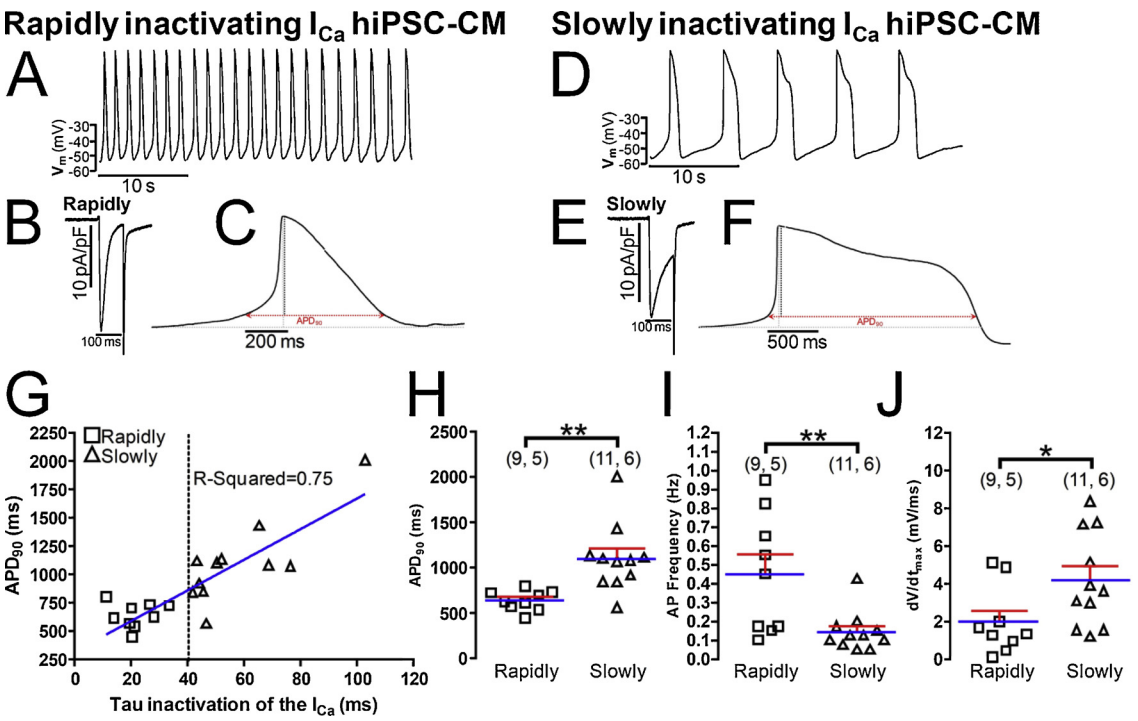


**Fig. 3.** Action potentials properties are correlated with the $I_{Ca}$ decay kinetics expressed in heterogeneous hiPSC-CMs populations. Panels A and D show examples of original traces of the action potentials (APs) spontaneously emitted during 35 s by hiPSC-CMs with rapidly or slowly inactivating $I_{Ca}$ respectively. Panels C and F exhibit two samples of singles APs obtained from cells with rapidly and slowly inactivating $I_{Ca}$ and panels B and E display the original $I_{Ca}$ records. Panel G shows a scatter-graph plot of the action potential duration at 90% repolarization ($APD_{90}$) (ms) vs. inactivation time constant ($\tau_i$) from hiPSC-CMs with rapidly (○) and slowly (●) inactivating $I_{Ca}$, hiPSC-CMs were classified as expressing rapidly- ($\tau_i \leq 40$ ms) or slowly-inactivating ($\tau_i > 40$ ms) L-type $Ca^{2+}$ channels. Panels H, I and J show the distribution of individual cell values and the average values (blue line) of $APD_{90}$, AP frequency (Hz) and AP upstroke velocity, dV/dt (mV/ms), respectively from hiPSC-CMs expressing rapidly (squares) or slowly (triangles) inactivating L-type $Ca^{2+}$ channels. In the panels H, I, and J, for each of the different data groups (rapidly or slowly inactivating $I_{Ca}$ cells), the number of cells ($n$) and the number of different cultures conducted to obtain these data (N) are indicated in parentheses as ($n$, N). Data were presented as the mean ± SEM in this figure. *$P < 0.05$; **$P < 0.01$; by unpaired two-tailed Student's t-test in this figure (For interpretation of the references to colour in this figure legend, the reader is referred to the web version of this article).

(39.5% ± 2.9%, Fig. 5B, vs. 52.30 ± 9.4%. Fig. 4D) than in $Ca^{2+}$ transporting channels, suggesting an additional calcium-dependent hypoxic suppressive effect. The mean inactivation time constant of $I_{Ba}$ in hiPSC-CMs was not significantly altered by hypoxia (Fig. 5D). In this set of 10 cells, 4 of them with rapidly inactivating $I_{Ca}$ in 2 mM $Ca^{2+}$ ($\tau_i < 40$ ms), increased their tau inactivation becoming slowly inactivating when the solution was replaced to normoxic $Ba^{2+}$ solutions (Fig. 5A, $\tau_i \geq 40$ ms). Even though in some of the slowly inactivating $I_{Ca}$ cells 2 mM $Ba^{2+}$ failed to increase the inactivation kinetics significantly (Fig. 5A), the amplitude of the current increased from ~40% to ~100% in all 10 cells, see panel A of Fig. 5 (the rapidly inactivating $I_{Ca}$ cell in 2 mM $Ca^{2+}$ with tau inactivation of 17.2 ms increased to 59.5 ms in 2 mM $Ba^{2+}$). The average suppressive effect of hypoxia in extracellular $Ba^{2+}$ was slightly smaller, but not significantly, in the rapidly inactivating $I_{Ca}$ cells (35.4 ± 5.7% *vs* 41.3 ± 3.8%), see red insert box in panel C of Fig. 5. These finding strongly support the assertion that the rapidly inactivating $I_{Ca}$ is not transported by T-type channels since the inactivation kinetics and current amplitude of the low threshold T-type channel are not significantly altered by replacing $Ca^{2+}$ with $Ba^{2+}$ [32,33].

Accordingly, the slow inactivation of the calcium channel, happening either innately in a population of hiPSC-CMs, or induced by transport of $Ba^{2+}$ through the channel appeared to sensitize the channel to hypoxia, suggesting that the rapid inactivation of the calcium channel, mediated by CDI, is protective against hypoxia.

### 3.2.3. *Regulation of the phosphorylated L-type calcium channels by hypoxia in cells with rapidly or slowly inactivating $I_{Ca}$*

Phosphorylation of the carboxyl tail of the α1C and β-subunits of the L-type calcium channel by PKA is known to facilitate $I_{Ca}$ [34,35]. Fig. 6 shows that 100 nM isoproterenol (ISO) increased $I_{Ca}$ by 90.21 ± 36.72% in the cells with rapidly inactivating $I_{Ca}$ (Fig. 6C) and by 86.48 ± 27.97% in the cells with slowly inactivating $I_{Ca}$ (Fig. 6D). In isoproterenol treated hiPSC-CMs hypoxia suppressed $I_{Ca}$ by 37.57 ± 23.16% in cells expressing the rapidly inactivating $I_{Ca}$ (Fig. 6C) and by 51.39 ± 23.86% in cells with slowly inactivating $I_{Ca}$ (Fig. 6D). Note that ISO not only did not protect against hypoxia in either cell type, but in fact enhanced the effect of hypoxia on the rapidly inactivating $I_{Ca}$ cells (37.5 ± 23.1% suppression in ISO treated cells, Fig. 6C, *vs.* 16.7 ± 2.6% suppression in control cells Fig. 4C, see also the effect of only hypoxia after ISO washout on the time course of the current., Fig. 6 C, 11.9 ± 6.3% $I_{Ca}$ suppression).

The hypoxia effects were also examined on the kinetics of inactivation of $I_{Ca}$ in phosphorylated and control cells (Fig. 6E and F). The data suggests that ISO significantly reduced $\tau_i$ in phosphorylated slowly inactivating $I_{Ca}$ hiPSC-CMs under normoxic conditions, but had no effect under hypoxic conditions (Fig. 6B and F). A positive linear correlation ($r = 0.6394$, $p < 0.001$) was found between the degree of hypoxic suppression of $I_{Ca}$ and the rate of its inactivation (scatter-gram and red correlation line, Fig. 6E), despite the great variability in the hypoxic suppressive effect between the two cell types. Thus, we conclude that PKA-mediated phosphorylation does not protect the channel against the suppressive effects of hypoxia in hiPSC-CMs. These results are consistent with those reported in adult rat cardiomyocytes [17,18] or in rN-CMs [19] and contrasts sharply with those described for adult guinea pig cardiomyocytes [36].

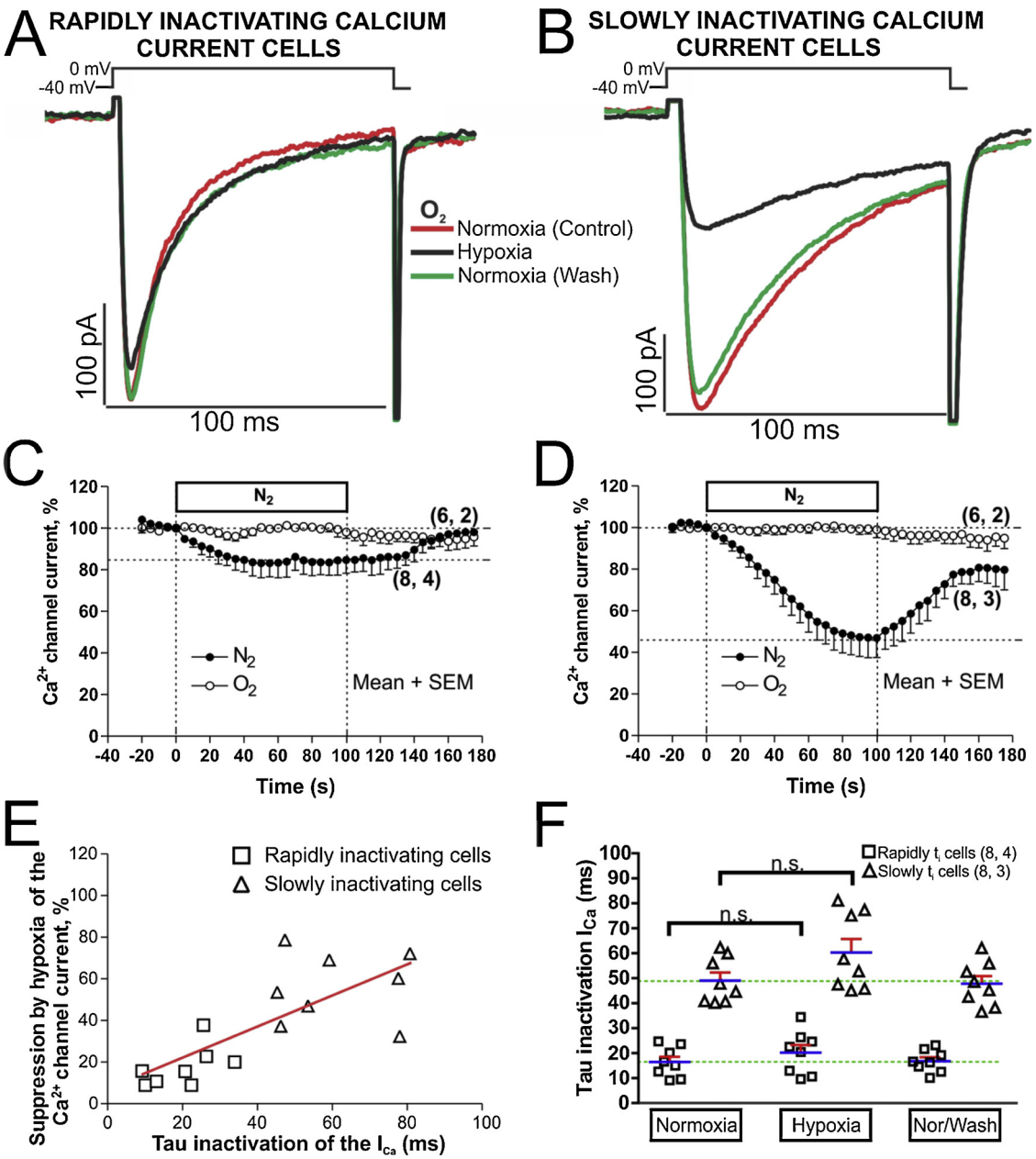


**Fig. 4.** Acute hypoxia differentially affects to the hiPSC-CMs with rapidly or slowly inactivating $I_{Ca}$. Panels A and B show examples of original traces of calcium currents obtained from two different hiPSC-CMs, activated by depolarization from -40 mV to 0 mV, exhibiting different rates of inactivation as well as differing degrees of suppression during acute hypoxia (black traces). Panels C and D display time courses of suppression of $I_{Ca}$ during 2 min of hypoxia stimulus ($N_2$ top bar, black circles) in hiPSC-CMs with rapidly and slowly inactivating $I_{Ca,}$ respectively. Time courses with white circles represent a set of hiPSC-CMs under normoxic condition during 200 s. Panel E shows a scatter-graph of hypoxic suppression of $I_{Ca}$ vs. inactivation time constant ($\tau_i$) from hiPSC-CMs with rapidly (□) and slowly (Δ) inactivating $I_{Ca}$ with the correlation line associate represented in red. Panel F show in a dot plot format the distribution of individual cell values and the average $\tau_i$ values of $I_{Ca}$ (blue line) before, during, and after exposure to hypoxia for each of the two cell types. In the panels C, D, and F, for each one of the different data groups, the number of cells (*n*) and the number of different cultures conducted to obtain these data (N) are indicated in parentheses as (*n*, N). Data were presented as the mean ± SEM in this figure. n.s.: not significant; by paired two-tailed Student's t-test in this figure (For interpretation of the references to colour in this figure legend, the reader is referred to the web version of this article).

### *3.3. Effects of acidification and ischemia (hypoxia plus acidosis) on rapidly and slowly inactivating hiPSC-CMs*

Because episodes of ischemia result not only in tissue hypoxia, but also to acidosis due to lactic acid accumulation [37], in another set of experiments we measured the combined effects of acute acidification and hypoxia. The combined effects of hypoxia plus acidosis were studied as to approximate "*ischemia*" in our hiPS-derived CMs. After 5 s of acidosis (pH, 6.7) $I_{Ca}$ was suppressed faster and by a greater degree in rapidly- than the slowly-inactivating $I_{Ca}$ cells; 22.13 ± 8.63% vs. 6.42 ± 3.17%, Fig. 7B and F. In both cases suppression of $I_{Ca}$ continued for ~50 s until steady-state levels were achieved. The final suppressive effects of acidosis were larger, but not significantly, in rapidly inactivating $I_{Ca}$ cell-type (37.85 ± 5.95% vs. 25.76 ± 4.83%), Fig. 7A, E, C and G.

The suppressive effect of ischemia (100 s of combined acidosis and hypoxia) on $I_{Ca}$ were similar in magnitude in both cells types, 45.14 ± 5.42% in rapidly inactivating $I_{Ca}$ vs. 47.7 ± 4.28% in slowly inactivating $I_{Ca}$ (pink trace records of the Fig. 7A, E and panels B, C, F and G of Fig. 7). Unexpectedly, the combined effects of acidosis and

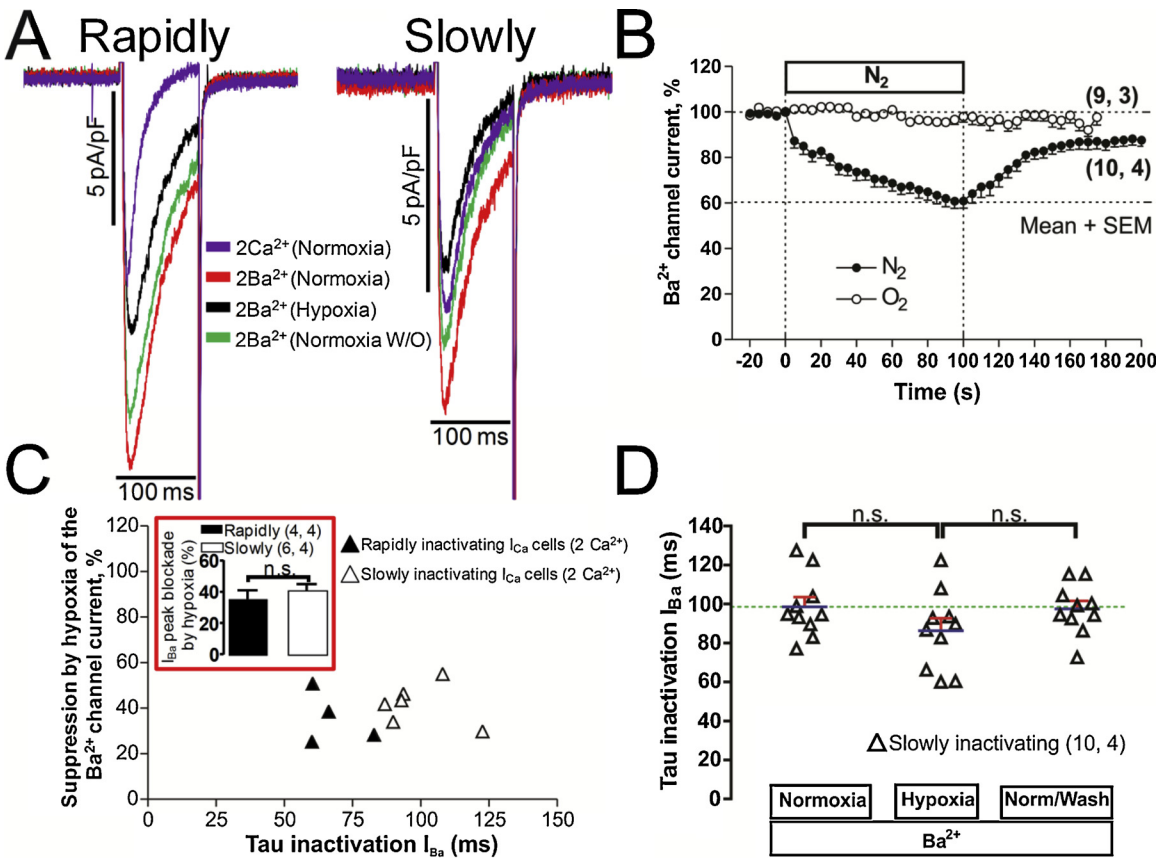


**Fig. 5.** Cardiac L-type $Ca^{2+}$ channel suppression by acute hypoxia whit $Ba^{2+}$ as charge carrier. Panels A show examples of original traces of rapidly and slowly inactivating $I_{Ca}$ hiPSC-CMs in the presence of 2 mM $Ca^{2+}$ (purple) that becomes slowly inactivating when we shifted the extracellular charge carrier to 2 mM $Ba^{2+}$ in normoxia condition (red traces). The cells were activated by depolarization from -40 mV to 0 mV and exposed to acute hypoxia (black traces) and normoxia washout (green traces). Panel B displayed the time course of suppression of $I_{Ba}$ during 100 s by hypoxia stimulus ($N_2$ top bar) in a set of hiPSC-CMs. Panel C shows a scattergraph plot of the hypoxic suppression degree of $I_{Ba}$ vs. inactivation time constant ($\tau_i$) of $I_{Ba}$ traces from hiPSC-CMs just after 100 s of hypoxia, with black or white triangles are distinguished the cells that have rapidly or slowly inactivating $I_{Ca}$ in the presence of 2 mM $Ca^{2+}$, the red insert box represent the average blockade by hypoxia in the presence of extracellular $Ba^{2+}$ in cells with rapidly or slowly inactivating $I_{Ca}$. Panel D show, in dot plot format, the distribution of individual cell values and the average $\tau_i$ values of $I_{Ba}$ (blue line) before, during, and after exposure to hypoxia. In the panels B, C and D, for each one of the different data groups, the number of cells (*n*) and the number of different cultures conducted to obtain these data (N) are indicated in parentheses as (*n*, N). Data were presented as the mean ± SEM in this figure. n.s.: not significant; by paired two-tailed Student's t-test in this figure. (For interpretation of the references to colour in this figure legend, the reader is referred to the web version of this article).

hypoxia were not additive in the slowly inactivating $I_{Ca}$ cells as they were in rapidly inactivating hiPSC-CMs (Fig. 7C, *vs.* 7 G).

### *3.4. Hypoxia and acidosis effects on global and focal $Ca^{2+}$ signaling in hiPSC-CMs*

The effects of acute hypoxia and acidosis on global and focal cytosolic $Ca^{2+}$ transients were also measured using Fluo-4 AM and GCamP6-FKBP targeted to RyR2 microdomains. $Ca_i$-transits were triggered by 100 ms depolarizing pulses followed by 1 s rapid puff of 3 mM caffeine. The rise of global cytosolic $Ca^{2+}$ by caffeine and the integration of the activated $Na^+$-$Ca^{2+}$ exchange current, $I_{NCX}$, [38] provided two estimates of SR calcium content. $I_{Ca}$, $I_{NCX}$, focal RyR2 μ-domain (GCaMP6-FKBP signals), the global cytosolic $Ca^{2+}$ transients (Fluo-4 AM signals), and the diastolic $[Ca^{2+}]_i$ (baseline fluorescence, $F_o$) were all measured and quantified as fluorescent ratios.

a) *Global cytosolic $Ca^{2+}$*: The global diastolic $Ca^{2+}$ levels of the rapidly and slowly inactivating $I_{Ca}$ hiPSC-CMs were not significantly different (~0.3-0.4 vs ~ 0.25-0.35 arbitrary fluorescence units– AFU– respectively), and acidosis or hypoxia did not seem to alter the diastolic $Ca^{2+}$ significantly (Fig. S3, traces C, D, I, J, and panel E and K). Global systolic $Ca_i^{2+}$ transients, though similar in the two cell types, were marginally higher in the slowly inactivating $I_{Ca}$ cells (~0.10-012 vs ~0.07-0.10 AFU, Fig. S3, tracings C, D, I, J and panels F and L). Acidosis decreased the global systolic $[Ca^{2+}]_i$ slightly. There was a tendency for larger effects in the rapidly inactivating $I_{Ca}$ cells (25.0% vs 20.2%, compare traces C & D and panel F of Fig. S3). Hypoxia, on the other hand, was more effective in suppressing the systolic $Ca_i^{2+}$ transients in the slowly inactivating compared to rapidly inactivating $I_{Ca}$ cells (35.1% vs. 19.2%, traces I, J and panel L of Fig. S3), consistent with the suppressive effect of hypoxia on $I_{Ca}$ (36.6% vs. 20.9%, tracings G, H and panel L, of Fig. S3). It is critical to note that in the latter set of experiments, cells were incubated in Fluo-4 AM, which is likely to have altered the $Ca^{2+}$ buffering capacity of the cells, and as such the effects of hypoxia and acidosis maybe dampened as compared to the set of experiments where the perforated patch clamp technique was used to monitor $I_{Ca}$ (Figs. 4 & 7).

b) *Focal $Ca^{2+}$ transients*: Diastolic $Ca^{2+}$ levels, measured in RyR2 μ-domains using GCamP6-FKBP, were slightly but not significantly higher in rapidly inactivating $I_{Ca}$ cells, (Fig. S4, traces C&G), and acidosis or hypoxia did not substantially modify this parameter in either cell type (Fig. S4 and S5, traces C, G and panel J). In marked contrast, however, acidosis substantially (37%) reduced the systolic GCaMP6-FKBP $Ca^{2+}$ signals in both cell types (Fig. S4, traces C, G

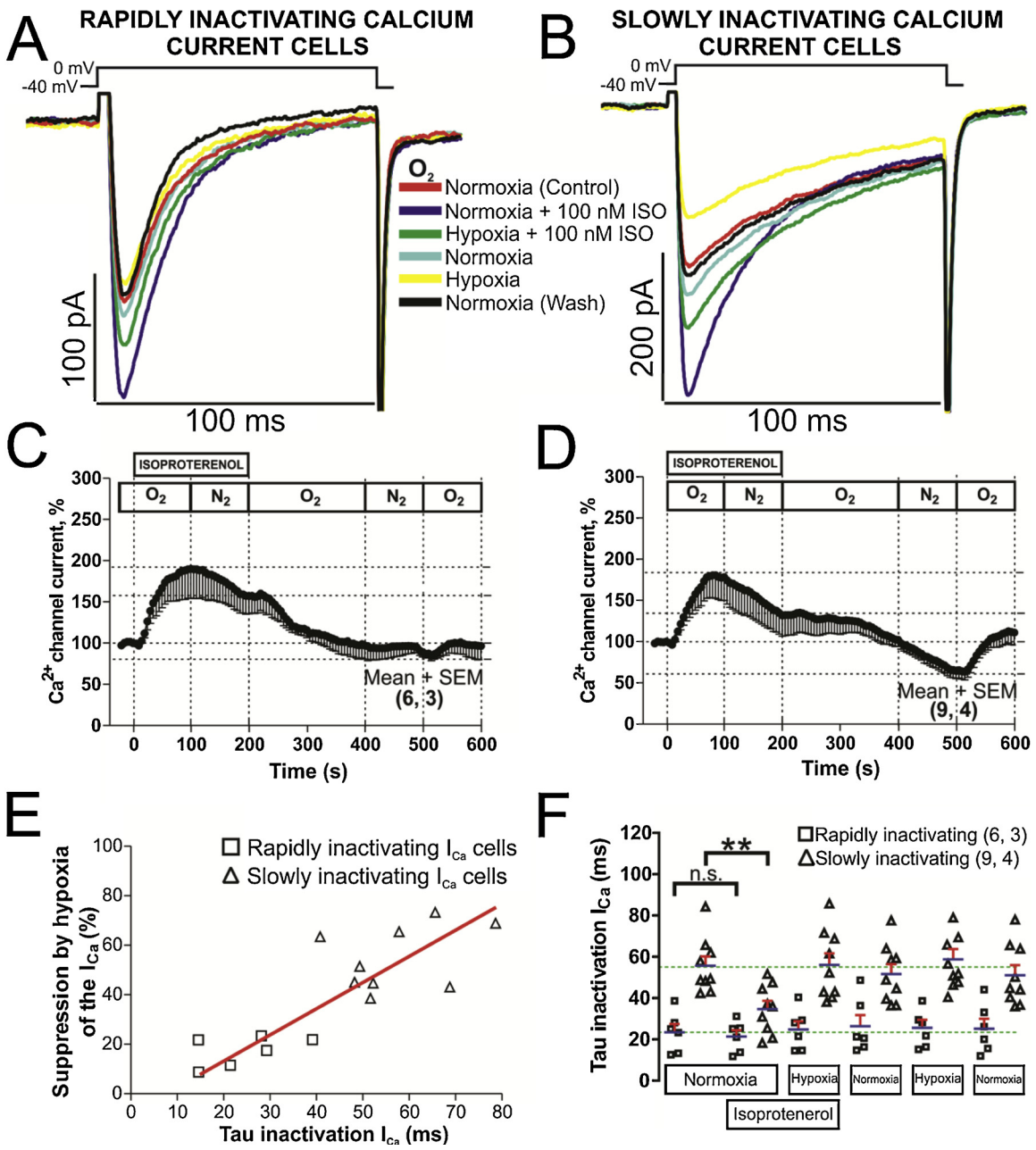


**Fig. 6.** Phosphorylation effects of isoproterenol (ISO) on calcium channels of hiPSC-CMs with rapidly or slowly inactivating $I_{Ca}$ in normoxia and hypoxia conditions. Panels A and B show examples of original traces of rapidly and slowly inactivating $I_{Ca}$ respectively, obtained from two different hiPSC-CMs, activated by depolarization from -40 mV to 0 mV and exposed to the following consecutive treatments: 1) red traces, normoxia control condition; 2) dark blue traces, initial treatment with 100 nM ISO in normoxia; 3) green traces, shift to the hypoxic condition maintaining the ISO treatment; 4) light blue traces, return to the normoxia condition after ISO washout; 5) yellow traces, second subsequent hypoxia stimulation without ISO, 6) black traces, final return to the normoxia condition. Panels C and D displayed time courses (in hiPSC-CMs with rapidly and slowly inactivating $I_{Ca}$, respectively) of modulation of $I_{Ca}$ by ISO perfused during 200 s (ISO bar) at the consecutives conditions of normoxia and hypoxia, represented by the sequence of $O_2$ and $N_2$ top bars, respectively. Panel E shows a scatter-graph plot of hypoxic suppression of $I_{Ca}$ vs. $\tau_i$ from hiPSC-CMs with rapidly (□) and slowly (Δ) inactivating $I_{Ca}$ with the respective correlation line found represented in red. Panel F shows, in a dot plot format, the distribution of individual cell values and the average $\tau_i$ values of $I_{Ca}$ (blue lines with SEM represented by red error bars) under normoxic and hypoxic conditions with or without ISO for each of the two cell types. Note here that the plotted data in the temporary course have a consider standard error of the mean (SEM) during the ISO treatment in both cell types due to the large variability that has ISO enhancing $I_{Ca}$ in hiPSC-CMs (different aspect as we found in rN-CMs) and how this error is reduced as the washout of the ISO progresses (final part of the temporary course of the panels C and D). In the panels C, D, and F, for each one of the different data groups, the number of cells (*n*) and the number of different cultures conducted to obtain these data (N) are indicated in parentheses as (*n*, N). Data were presented as the mean ± SEM in this figure. $^{**}P < 0.01$; n.s.: not significant; by paired two-tailed Student's *t*-test in this figure. Mann-Whitney rank-sum test. (For interpretation of the references to colour in this figure legend, the reader is referred to the web version of this article).

and panel I). $I_{Ca}$ density was similarly suppressed by acidosis in the rapidly and slowly inactivating $I_{Ca}$ cells (30% vs 23% respectively, Fig. S4, traces A, E and panel I). There was no or little difference in the $Ca^{2+}$ content of the SR, calculated from the integral of the caffeine-induced $I_{NCX}$ (~0.6 to 0.8 × $10^{-12}$ M), in the two cell types (Fig. S4 L), and was reduced similarly on exposure to 100 s of acidosis by 35% in both cell types (Fig. S4 B, F and L). On the other hand, hypoxia differentially suppressed the systolic GCaMP6-FKBP

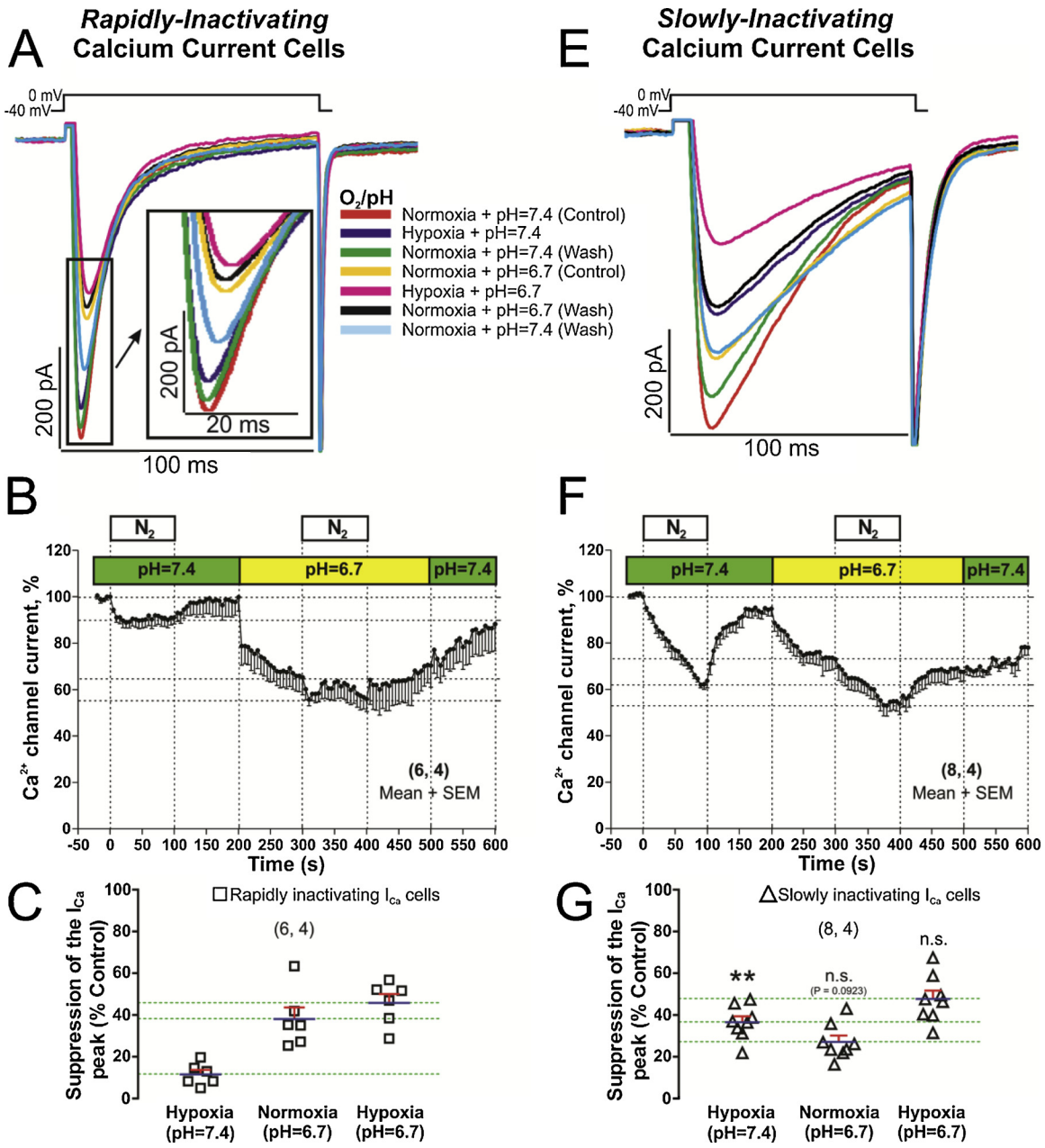


**Fig. 7.** L-type $Ca^{2+}$ channel is differentially blocked in hiPSC-CMs with rapidly or slowly inactivating $I_{Ca}$ when the stimulus of acute hypoxia and acidification are combined. Panels A and E show examples of original traces of rapidly and slowly inactivating $I_{Ca}$ respectively, obtained from two different hiPSC-CMs, activated by depolarization from -40 mV to 0 mV and exposed to the following consecutive treatments: 1) red traces, normoxia and pH (7.4) control condition; 2) dark blue traces, hypoxia and control pH 7.4; 3) green traces, back to the initial control treatment (normoxia and pH 7.4); 4) yellow traces, normoxia and low pH 6.7; 5) pink traces, hypoxia and acidosis combined; 6) black traces, back to normoxia and pH 6.7; 7) light blue traces, washout period to normoxia and pH 7.4. Panels B and F displayed time courses (in hiPSC-CMs with rapidly and slowly inactivating $I_{Ca}$ respectively) of the $I_{Ca}$ suppression by acidosis (pH = 6.7 bar) and/or hypoxia ($N_2$ bar). Panels C and G represents, in dot plots format, the distribution of individual cell values and the average of $I_{Ca}$ blocked (blue lines with SEM represented by red error bars) by hypoxia, acidosis, and both interventions together for both cell types. In the panels B, C, F and G, for each one of the different data groups, the number of cells (*n*) and the number of different cultures needed to obtain these data (N) are indicated in parentheses as (*n*, N). Data were presented as the mean ± SEM in this figure. Differences between rapidly and slowly inactivating $I_{Ca}$ cells in hypoxia, acidosis and both stimuli together. $^{**}P < 0.01$; n.s.: not significant; by unpaired two-tailed Student's t-test. (For interpretation of the references to colour in this figure legend, the reader is referred to the web version of this article).

$Ca^{2+}$ signals in the two cell types (25% in the rapidly vs 45% in the slowly inactivating $I_{Ca}$ cells), panels C, G and panel I, Fig. S5. This differential effect may reflect the differences in $I_{Ca}$ suppressive effect of hypoxia on the slowly inactivating $I_{Ca}$ cell type (42% vs 16% in the rapidly inactivating $I_{Ca}$ cells), compare panels A, E and I, of figure S5. The $Ca^{2+}$ content of SR was also suppressed by 100 s exposure to hypoxia to a greater degree in the slowly inactivating $I_{Ca}$ cells (50% vs 26% in rapidly inactivating $I_{Ca}$ hiPSC-CMs), Fig. S5 B, F and L. Similar reductions in the SR $Ca^{2+}$ store were also noted when the store content was quantified by measurements of fluorescence of GCamP6-FKBP signals (panel K, tracings D, H of Fig. S5).

## 4. Discussion

Human fibroblast derived developing cardiomyocytes grown in cultures, express two cell types based on the kinetics of inactivation of

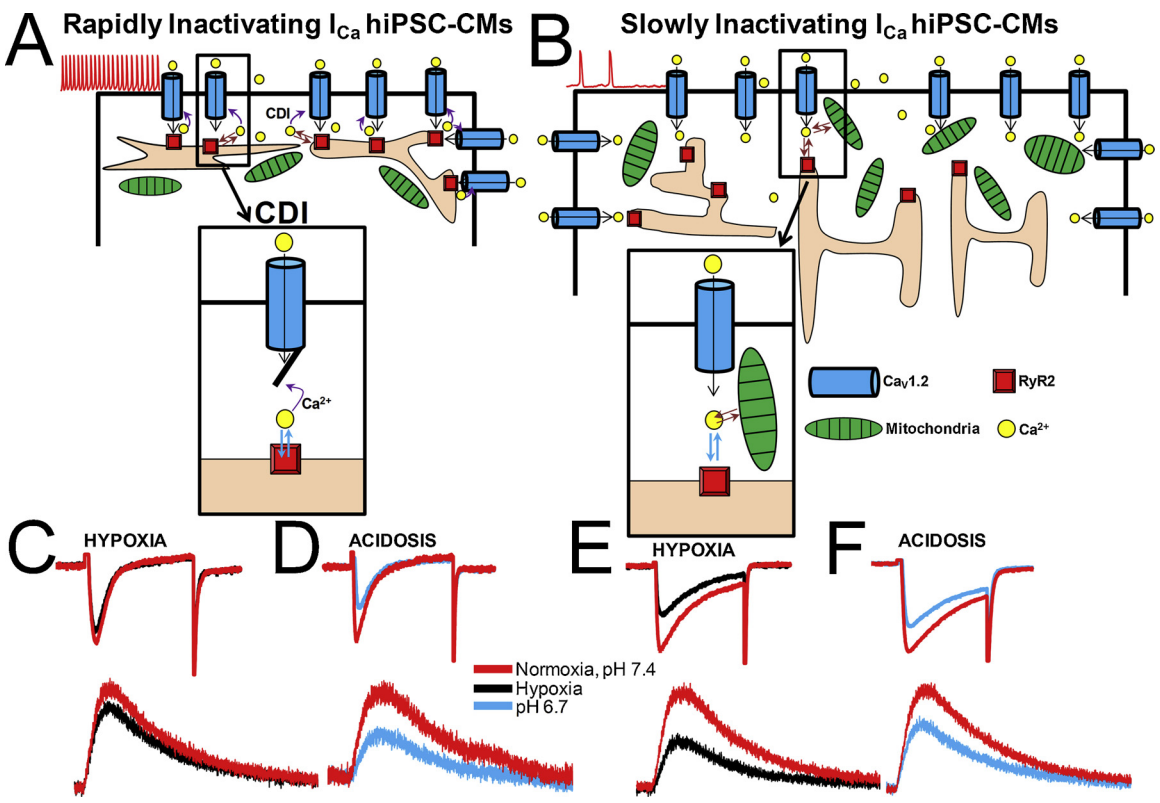


**Scheme 1.** $Ca^{2+}$ handling by hiPSC-CMs during acute hypoxia and acidosis. Two cell-type populations of hiPSC-CMs were identified based on the kinetics of $I_{Ca}$ inactivation during growth in culture. Smaller, 3-4days hiPSC-CMs expressed predominantly rapidly inactivating $I_{Ca}$ (panel A), shorter action potentials, faster spontaneous pacing rates, whereas larger 6–8days hiPSC-CMs expressed mostly slowly inactivating $I_{Ca}$ (panel B) and showed wider APs and slower spontaneous pacing rates ("*Ventricular type APs*"). Acute hypoxia suppress $I_{Ca}$ to a greater degree in slowly inactivating $I_{Ca}$ hiPSC-CMs (~40%, panel E) compared to rapidly inactivating $I_{Ca}$ cells (~15%, panel C). Suppressive effect of acute acidosis on $I_{Ca}$ (~35%, pH 6.7) was not cell-type dependent (panel D and F). Focal RyR2 $Ca^{2+}$ microdomains were suppressed in a similar range to $I_{Ca}$ inhibition. Acute hypoxia suppresses $I_{Ca}$ in *rapidly inactivating* cell population by a mechanism involving $Ca^{2+}$-dependent inactivation (insert in panel A), while mitochondrial $Ca^{2+}$ uptake may also contribute to $I_{Ca}$ suppression in *slowly inactivating* cell population (insert in panel B).

their L-type $Ca^{2+}$ channels. This finding may, in part, be responsible for the heterogeneity of action potential duration observed by many investigators working in this field and taken as evidence for the ancestral heterogeneity of hiPSC-CM cultures expressing atrial, ventricular, and conduction tissue cell-types. While the suppressive effects of hypoxia on $I_{Ca}$ depended critically on the cell type expressing slowly or rapidly inactivating $Ca^{2+}$ channels, acidosis effects were independent of cell types. The stronger suppressive effects of hypoxia on slowly inactivating $I_{Ca}$ cells was consistent with the idea that $Ca^{2+}$ dependent inactivation protects the channel against hypoxic suppression (Scheme 1), somewhat similar to that found in adult and neonatal rat cardiomyocytes where suppression of CDI by $Ba^{2+}$ [17–19], or $Ca^{2+}$ overbuffering [19] enhanced the hypoxia's suppressive effects. Unexpectedly, hypoxia was more effective in suppressing $Ca^{2+}$ signaling measured at the RyR2 micro-domains rather than in global cytosolic space, suggesting variable effects of hypoxia on calcium signaling pathway.

### 4.1. Development of rapidly and slowly inactivating $I_{Ca}$ in hiPSC-CMs cultures

In early 4 day cultures of hiPSC-CMs, $I_{Ca}$ magnitude was small and cultures contained similar percentages of rapidly and slowly inactivating L-type $I_{Ca}$ cells (Fig. 1A, C, and D). In older 7–8 day cultures, as the magnitude of $I_{Ca}$ and cell size increased, the cultures appeared to express mostly the slowly inactivating $I_{Ca}$ cell types (Fig. 1B, C and D). This finding is somewhat similar to those of neonatal rat cardiomyocytes where the first 5 days cultures express predominately the rapidly inactivating L-type $I_{Ca}$ cells, while older cultures have predominantly the slowly inactivating $I_{Ca}$ cell types [19,39]. This is in sharp contrast to $I_{Ca}$ measured in one week old cultures of adult rat cardiomyocytes, where only rapidly inactivating L-type $I_{Ca}$ was measured [17,18].

Three possible mechanisms were considered to be responsible for the expression of the two kinetically different $I_{Ca}$ cell types: 1) a larger surface to volume ratio in smaller cells of early cultures, where $Ca^{2+}$ influx and release could be more effective in activating CDI than in the older cells with larger volumes (Scheme 1); 2) variable expression of molecular determinants of CDI (for instance, CaM, CaM-binding sites and the IQ-like domain) in developing hiPSC-CMs; and 3) culture-age dependent expression of $Ca_V1.2$ and $Ca_V1.3$. Since the inactivation kinetics of $I_{Ca}$ were similarly affected, in hiPSC-CMs with rapidly or slowly inactivating $I_{Ca}$, when $Ba^{2+}$ was the charge carrier through the $Ca^{2+}$ channels (Fig. 5C) and the tail-current deactivation kinetics of the two cell types were not significantly different (Fig. S1), variable expression of molecular determinants of CDI was considered unlikely. On the other hand, the linear correlation of cell size and the rate of $I_{Ca}$ inactivation, in more than 150 cells (Fig. 1H), supports the cell size and the ultrastructural proximity of $Ca^{2+}$ stores to plasma membrane as the more likely possibility, see also rN-CMs data [19].

The possibility that the two cardiomyocytes types resulted from differential expression of two calcium channel types, ($Ca_V1.2$ & $Ca_V1.3$), was also not supported by the finding that the level expression of $Ca_V1.2$ mRNA was markedly greater than $Ca_V1.3$ both in the early (day4) or late (day7) culture cells (Fig. S2). Additionally, the failure of the selective $Ca_V1.3$ antagonist (1-(3-chlorophenethyl)-3-cyclopentylpyrimidine-2,4,6-(1*H*,3*H*,5*H*)-trione) [30] to block $I_{Ca}$ in hiPSC-

CMs, where 2 or 10 μM nifedipine produced ~90-95% block of $I_{Ca}$ (panel D of Fig. 2), plus the effectiveness of low concentrations of nifedipine in equally suppressing the current in the two cell types, strongly supports the single rather than two channel types possibility (Fig. 2). Our findings suggest that only $Ca_V1.2$ subtype of L-type calcium channel is expressed in hiPSC-CMs producing 2-different kinetics of inactivation.

### 4.2. Regulation of calcium channels by hypoxia or acidosis in hiPSC-CMs

Although the consequences of hypoxia and acidosis on $I_{Ca}$ have been studied by a large number of labs in adult rat or guinea-pig ventricular myocytes [17,18,36,40–43] or in rN-CMs [19,44,45] very little information has been published about the combined effects of these interventions in modulating $I_{Ca}$ and calcium signaling, especially in hiPSC-CMs [46]. Fig. 4C, D shows that the suppressive effect of hypoxia on $I_{Ca}$ varied quantitatively in cells with rapidly or slowly inactivating $I_{Ca}$ (~15% vs. ~45%, respectively). Since the slowly inactivating $I_{Ca}$ hiPSC-CMs are more abundant at the end of first week in culture (~75% vs ~25%), hiPSC-CMs appear to be more vulnerable to acute hypoxia as compared to rA-CMs that express mostly the rapidly inactivating $I_{Ca}$ in the first week of development in culture, showing only ~10–20% hypoxic suppressive effect on $I_{Ca}$ [17,18]. This disparity in effects of hypoxia on hiPSC-CMs did not occur when $Ba^{2+}$ was the charge carrier through the $Ca^{2+}$ channel (Fig. 5), implying that CDI was critical in protecting against the hypoxic suppression of $I_{Ca}$. On the other hand, the suppressive effect of acidosis was significantly larger in rapidly inactivating $I_{Ca}$ hiPSC-CMs (~38% vs. ~26%, Fig. 7), in sharp contrast to that reported for rN-CMs where the acidosis suppressive effects were similar in both cell types. In both cell types, there was an initial fast suppression of $I_{Ca}$ in the first 5 s of exposure to acute acidosis, presumable caused by binding of protons to the $Ca^{2+}$ permeation site of the channel pore [47–49], and/or neutralizing the membrane surface charges and thereby altering the gating of the channel [50–52]. Note, that this effect was significantly larger in rapidly inactivating $I_{Ca}$ hiPSC-CMs (~22% vs. ~6%, Fig. 7B and F). The slow phase of acidosis suppression of $I_{Ca}$, following the initial rapid phase, could be the consequence of a smaller but continued acidification (~0.1 pH units) of intracellular milieu in perforated patch clamped conditions, secondary to extracellular acidification, previously reported [53–57].

Although the suppressive effects of ischemia (hypoxia plus acidosis) on $I_{Ca}$ of hiPSC-CMs were equivalent (~45%) in both cell types (Fig. 7B, C, F, G), there was an additive effect of hypoxia plus acidosis in only rapidly inactivating $I_{Ca}$, suggesting that in addition to blocking of the channel and heme-oxygenase activation [18], hypoxia may also suppress $I_{Ca}$ by metabolic inhibition of mitochondrial ATP hydrolysis leading to further intracellular acidosis [57,58] that additionally and differentially suppresses $I_{Ca}$ in the two cell types (Scheme 1). The quick and reversible suppressive effects of hypoxia when $Ba^{2+}$ is the charge carrier through the channel (Fig. 5A, B), seen also in rat cardiomyocytes [18,19,59], supports the idea that cardiac L-type $Ca^{2+}$ channel can sense $O_2$ directly through a mechanism independent of the time-dependent activation of, for instance, ROS, hypoxia-inducible factors (HIF), ADP or ATP. Even though the molecular nature of this rapid $O_2$ sensing mechanism remains not fully understood, the finding that heme-oxygenase 2 (HO-2) inhibitors block the suppressive effects of hypoxia on $I_{Ca}$ is consistent with the possibility that heme-oxgenase bound to CaM/CaMKII binding motif of C-carboxyl terminal of L-type $Ca^{2+}$ channel may render the channel $O_2$ sensitive [18]. The finding that specific inhibitors of HO-2 and CaMKII, similarly and reversibly suppressed $I_{Ca}$ in hiPSC-CMs as hypoxia, i.e. producing similar $I_{Ca}$ blocking pattern without additive effects (Fig. S6), suggests the same pathway might be involved in the $I_{Ca}$ suppression.

### 4.3. Acidosis and hypoxia modulation of calcium signaling

In hiPSC-CMs incubated with the Fluo-4 AM, to measure global cytosolic $Ca^{2+}$, acidosis or hypoxia had a proportional effect on $I_{Ca}$-triggered $Ca^{2+}$ release as expected from its direct suppressive effect on $I_{Ca}$ and CICR (Fig. S3,F, L), consistent with rN-CMs, where acidosis or hypoxia had a small effect on $I_{Ca}$-triggered $Ca^{2+}$ release [19]. On the other hand, in hiPSC-CMs infected with genetically engineered probes (GCaMP6-FKBP), to measure RyR2 $Ca^{2+}$ microdomains, acidosis (Fig. S5 I) alone suppressed the focal $Ca^{2+}$-transients to a greater extent than that expected from suppression of $I_{Ca}$. The average reduction in the SR $Ca^{2+}$ content, calculated from the integral of the caffeine-activated $I_{NCX}$, during acidosis or hypoxia (Figs. S4 L and S5 L) was proportional to the suppression of $I_{Ca}$ (Figs. S4 I and S5 I, lower dot plots) and its accompanying $Ca^{2+}$-transients (Figs. S4 I and S5 I, upper dot plots) for both cell types. Unexpectedly, only in the slowly inactivating $I_{Ca}$ hiPSC-CMs there was a significant reduction in the SR $Ca^{2+}$ content by acidosis and hypoxia (Figs. S4 L and S5 L). The suppression of focal $Ca^{2+}$, but not global $Ca^{2+}$, signals by hypoxia or acidosis appears to be consistent with suppressive effects of these interventions on SR $Ca^{2+}$ content and suggests that focal $Ca^{2+}$-transients may better represent the pathophysiological regulation of CICR. Extracellular acidosis also modulated $I_{Ca}$ gating and slowed the activation of $I_{Ca}$ in hiPSC-CMs (Fig. S3 A, B and S4 A, E) consistent with previous reports in rabbit and guinea pig ventricular myocytes [48,60,61] as it delayed the activation of $I_{NCX}$ and their corresponding calcium transients (Fig. S4B, D, F, H).

### 4.4. Beta-adrenergic modulation of hypoxic effects

In adult guinea pig ventricular cardiomyocytes, hypoxia enhances the affectability of the L-type $Ca^{2+}$ channel to the β-adrenergic agonists [36]. In sharp contrast in rN-CMs [19], or adult rat cardiomyocytes [17,18], isoproterenol application under hypoxic conditions enhanced $I_{Ca}$ suppression. In support of these results metabolic inhibition such as ischemia, almost completely suppressed $I_{Ca}$ that was enhanced by β-adrenergic agonist isoproterenol in adult frog cardiomyocytes [57]. In hiPSC-CMs even though ISO enhanced $I_{Ca}$ significantly (~90%) in both cell types (Fig. 6C, D), β-adrenergic phosphorylation did not protect the channel against hypoxia either in rapidly inactivating $I_{Ca}$ (~ 17% in control vs. ~37% suppression in ISO) or in slowly inactivating cell types (~50% suppression of $I_{Ca}$ in control or phosphorylated channels) Fig. 6. The phosphorylation of L-type $Ca^{2+}$ channel in normoxic conditions reduced significantly the $\tau_i$ of the $I_{Ca}$ (~36%) only in the slowly inactivating $I_{Ca}$ hiPSC-CMs, but hypoxia reversed this effect (Fig. 6A, B and F), this may result from β-adrenergic phosphorylation accelerating and synchronizing cardiac RyR2 response per unit of single L-type $Ca^{2+}$ channel [62], making CICR more efficient and enhancing CDI. Since rapidly inactivating $I_{Ca}$ hiPSC-CMs appear to be more resistant to hypoxia, it is likely that the enhancement of CDI may also desensitize the channel to hypoxia. It remains unclear as to why ISO has a significantly different time-dependent effect in culture of hiPSC-CMs (Fig. 1I) when the density of $I_{Ca}$ remains unchanged (Fig. 1E).

### 4.5. Physiological and biophysical implications

It is generally assumed that hiPSC-CM cultures have mixed cellular populations, representing atrial, ventricular, and conducting/pacemaker cells. These assumptions are primarily based on measured action potential morphologies: i.e. longer action potentials with prominent plateaus are assumed to be ventricular, while those with shorter plateau phases are identified as atrial, and those showing diastolic depolarization as pacemaker/conducting cells. In fact, this classification is arbitrary and might be misleading, because: 1) Recording of action potential using patch pipette is invasive and may critically alter the native intracellular milieu and create leaks and cellular run down. If the action potential is to be measured reliably, great care must be taken not to

introduce holding current from the amplifier, a difficult undertaking unless ultra-tight giga-seal is achieved in current-clamp recording mode [63–67]; 2) there is likely to be more than one cell population based on expression of rapidly and slowly inactivating $I_{Ca}$ (Fig. 1 and 3, Scheme 1); 3) variability in cell size, and juxtaposition of SR $Ca^{2+}$ store element *vis-a-vis* sarcolemmal $I_{Ca}$ will also affect the action potential morphology (Scheme 1); 4) The robust $Ca^{2+}$ signaling and very low expression of $Ik_1$ in hiPSC-CMs would trigger spontaneous beating characteristics that are often associated with pacemaking/conducting cells. Thus, the variability in action potential morphology is more likely to arise from variability in cellular morphology and $I_{Ca}$ kinetics, in part regulated by the intracellular $Ca^{2+}$ stores, than by the developmental origins of the myocytes (Scheme 1). In this sense, we present new evidence that heterogeneous hiPSC-CMs populations previously reported to reflect atrial and ventricular cell types based on the differences of their APs morphology are most likely caused by the $I_{Ca}$ decay kinetics in a homogenous, but growing cell population (Fig. 3), rather than cell ancestry.

Although differential expression of $Ca_V1.2$ and $Ca_V1.3$ could in part be responsible for the two cell-type populations described above, our pharmacological intervention as well as mRNA expression levels measurements do not support this possibility. The more likely possibility is the changes in cellular morphology and the expression levels of SR $Ca^{2+}$ stores with cell growth in culture vis-a-vis the surface membrane expression of $I_{Ca}$ that produces the two cell populations [19,68–71]. This and previously published works suggest that $Ca^{2+}$ dependent inactivation protects the channel against hypoxic suppression. This mechanism is not only regulated by the proximity of SR $Ca^{2+}$ pools to the sarcolemmal L-type $Ca^{2+}$ channels, but also by the mitochondria contribution to the intracellular calcium homeostasis that critically determines the variability of inactivation kinetics and thereby the degree to which the myocyte is affected by hypoxia.

## Author contributions

Designed the experiments: M. Morad.

*Conducted experiments and analysis:* Jose-Carlos Fernandez-Morales, Wei Hua, Yuyu Yao.

*Wrote the manuscript:* Jose-Carlos Fernandez-Morales, and M. Morad.

## Author disclosure statement

No conflicts of interest, financial or otherwise, are declared by the author(s).

## Declaration of interest statement

No conflicts of interest, financial or otherwise, are declared by the author(s).

## Acknowledgments

We thank Brittany Henry for general technical help. This work was supported by the National Institute of Health grants to M.M.: (1) NIHR01 HL15162, (2) NIHR01 HL107600.

## Appendix A. Supplementary data

Supplementary material related to this article can be found, in the online version, at doi:https://doi.org/10.1016/j.ceca.2018.12.006.

## References

[1] G.A. Roth, C. Johnson, A. Abajobir, F. Abd-Allah, S.F. Abera, G. Abyu, M. Ahmed, B. Aksut, T. Alam, K. Alam, F. Alla, N. Alvis-Guzman, S. Amrock, H. Ansari, J. Arnlov, H. Asayesh, T.M. Atey, L. Avila-Burgos, A. Awasthi, A. Banerjee, A. Barac, T. Barnighausen, L. Barregard, N. Bedi, E. Belay Ketema, D. Bennett, G. Berhe, Z. Bhutta, S. Bitew, J. Carapetis, J.J. Carrero, D.C. Malta, C.A. Castaneda-Orjuela, J. Castillo-Rivas, F. Catala-Lopez, J.Y. Choi, H. Christensen, M. Cirillo, L. Cooper Jr., M. Criqui, D. Cundiff, A. Damasceno, L. Dandona, R. Dandona, K. Davletov, S. Dharmaratne, P. Dorairaj, M. Dubey, R. Ehrenkranz, M. El Sayed, E.J.A. Zaki, A. Faraon, T. Esteghamati, M. Farid, V. Farvid, E.L. Feigin, G. Ding, T. Fowkes, R. Gebrehiwot, A. Gillum, P. Gold, R. Gona, T.D. Gupta, N. Habtewold, T. Hafezi-Nejad, G.B. Hailu, G. Hailu, H.Y. Hankey, K.H. Hassen, R. Abate, S.I. Havmoeller, M. Hay, P.J. Horino, K. Hotez, S. Jacobsen, M. James, P. Javanbakht, D. Jeemon, J. John, Y. Jonas, C. Kalkonde, A. Karimkhani, Y. Kasaeian, A. Khader, Y.H. Khan, S. Khang, A.T. Khera, J. Khoja, D. Khubchandani, D. Kim, S. Kolte, K.J. Kosen, G.A. Krohn, G.F. Kumar, D.K. Kwan, A. Lal, S. Larsson, A. Linn, P.A. Lopez, H.M.A. Lotufo, Razek El, R. Malekzadeh, M. Mazidi, T. Meier, K.G. Meles, G. Mensah, A. Meretoja, H. Mezgebe, T. Miller, E. Mirrakhimov, S. Mohammed, A.E. Moran, K.I. Musa, J. Narula, B. Neal, F. Ngalesoni, G. Nguyen, C.M. Obermeyer, M. Owolabi, G. Patton, J. Pedro, D. Qato, M. Qorbani, K. Rahimi, R.K. Rai, S. Rawaf, A. Ribeiro, S. Safiri, J.A. Salomon, I. Santos, M. Santric Milicevic, B. Sartorius, A. Schutte, S. Sepanlou, M.A. Shaikh, M.J. Shin, M. Shishehbor, H. Shore, D.A.S. Silva, E. Sobngwi, S. Stranges, S. Swaminathan, R. Tabares-Seisdedos, N. Tadele Atnafu, F. Tesfay, J.S. Thakur, A. Thrift, R. Topor-Madry, T. Truelsen, S. Tyrovolas, K.N. Ukwaja, O. Uthman, T. Vasankari, V. Vlassov, S.E. Vollset, T. Wakayo, D. Watkins, R. Weintraub, A. Werdecker, R. Westerman, C.S. Wiysonge, C. Wolfe, A. Workicho, G. Xu, Y. Yano, P. Yip, N. Yonemoto, M. Younis, C. Yu, T. Vos, M. Naghavi, C. Murray, Global, regional, and national burden of cardiovascular diseases for 10 causes, 1990 to 2015, J. Am. Coll. Cardiol. 70 (2017) 1–25.

[2] N. Kawaguchi, T. Nakanishi, Cardiomyocyte regeneration, Cells 2 (2013) 67–82.

[3] S.R. Braam, R. Passier, C.L. Mummery, Cardiomyocytes from human pluripotent stem cells in regenerative medicine and drug discovery, Trends Pharmacol. Sci. 30 (2009) 536–545.

[4] K. Rajala, M. Pekkanen-Mattila, K. Aalto-Setala, Cardiac differentiation of pluripotent stem cells, Stem Cells Int. 2011 (2011) 383709.

[5] C.W. Don, C.E. Murry, Improving survival and efficacy of pluripotent stem cell-derived cardiac grafts, J. Cell. Mol. Med. 17 (2013) 1355–1362.

[6] D.M. Bers, Cardiac excitation-contraction coupling, Nature 415 (2002) 198–205.

[7] X.H. Zhang, S. Haviland, H. Wei, T. Saric, A. Fatima, J. Hescheler, L. Cleemann, M. Morad, Ca2+ signaling in human induced pluripotent stem cell-derived cardiomyocytes (iPS-CM) from normal and catecholaminergic polymorphic ventricular tachycardia (CPVT)-afflicted subjects, Cell Calcium 54 (2013) 57–70.

[8] S. Li, H. Cheng, G.F. Tomaselli, R.A. Li, Mechanistic basis of excitation-contraction coupling in human pluripotent stem cell-derived ventricular cardiomyocytes revealed by $Ca^{2+}$ spark characteristics: direct evidence of functional $Ca^{2+}$-induced $Ca^{2+}$ release, Heart Rhythm 11 (2014) 133–140.

[9] X.H. Zhang, H. Wei, T. Saric, J. Hescheler, L. Cleemann, M. Morad, Regionally diverse mitochondrial calcium signaling regulates spontaneous pacing in developing cardiomyocytes, Cell Calcium 57 (2015) 321–336.

[10] R.W. Hadley, W.J. Lederer, $Ca^{2+}$ and voltage inactivate $Ca^{2+}$ channels in guinea-pig ventricular myocytes through independent mechanisms, J. Physiol. 444 (1991) 257–268.

[11] M.A. van der Heyden, T.J. Wijnhoven, T. Opthof, Molecular aspects of adrenergic modulation of cardiac L-type $Ca^{2+}$ channels, Cardiovasc. Res. 65 (2005) 28–39.

[12] J. Striessnig, N.J. Ortner, A. Pinggera, Pharmacology of L-type calcium channels: novel drugs for old targets? Curr. Mol. Pharmacol. 8 (2015) 110–122.

[13] C. Bauwens, T. Yin, S. Dang, R. Peerani, P.W. Zandstra, Development of a perfusion fed bioreactor for embryonic stem cell-derived cardiomyocyte generation: oxygen-mediated enhancement of cardiomyocyte output, Biotechnol. Bioeng. 90 (2005) 452–461.

[14] S. Niebruegge, C.L. Bauwens, R. Peerani, N. Thavandiran, S. Masse, E. Sevaptisidis, K. Nanthakumar, K. Woodhouse, M. Husain, E. Kumacheva, P.W. Zandstra, Generation of human embryonic stem cell-derived mesoderm and cardiac cells using size-specified aggregates in an oxygen-controlled bioreactor, Biotechnol. Bioeng. 102 (2009) 493–507.

[15] R.E. Horton, D.T. Auguste, Synergistic effects of hypoxia and extracellular matrix cues in cardiomyogenesis, Biomaterials 33 (2012) 6313–6319.

[16] C. Correia, M. Serra, N. Espinha, M. Sousa, C. Brito, K. Burkert, Y. Zheng, J. Hescheler, M.J. Carrondo, T. Saric, P.M. Alves, Combining hypoxia and bioreactor hydrodynamics boosts induced pluripotent stem cell differentiation towards cardiomyocytes, Stem Cell Rev. 10 (2014) 786–801.

[17] S. Movafagh, M. Morad, L-type calcium channel as a cardiac oxygen sensor, Ann. N. Y. Acad. Sci. 1188 (2010) 153–158.

[18] A.O. Rosa, S. Movafagh, L. Cleemann, M. Morad, Hypoxic regulation of cardiac $Ca^{2+}$ channel: possible role of haem oxygenase, J. Physiol. 590 (2012) 4223–4237.

[19] J.C. Fernandez-Morales, M. Morad, Regulation of Ca(2+) signaling by acute hypoxia and acidosis in rat neonatal cardiomyocytes, J. Mol. Cell. Cardiol. 114 (2018) 58–71.

[20] K. Si-Tayeb, F.K. Noto, A. Sepac, F. Sedlic, Z.J. Bosnjak, J.W. Lough, S.A. Duncan, Generation of human induced pluripotent stem cells by simple transient transfection of plasmid DNA encoding reprogramming factors, BMC Dev. Biol 10 (2010) 81.

[21] X. Lian, J. Zhang, S.M. Azarin, K. Zhu, L.B. Hazeltine, X. Bao, C. Hsiao, T.J. Kamp, S.P. Palecek, Directed cardiomyocyte differentiation from human pluripotent stem cells by modulating Wnt/beta-catenin signaling under fully defined conditions, Nat. Protoc. 8 (2013) 162–175.

[22] M. Lindau, J.M. Fernandez, A patch-clamp study of histamine-secreting cells, J. Gen. Physiol. 88 (1986) 349–368.

[23] R. Horn, A. Marty, Muscarinic activation of ionic currents measured by a new whole-cell recording method, J. Gen. Physiol. 92 (1988) 145–159.

[24] P.J. Aggett, P.K. Fenwick, H. Kirk, The effect of amphotericin B on the permeability of lipid bilayers to divalent trace metals, Biochim. Biophys. Acta 684 (1982) 291–294.
[25] J. Rae, K. Cooper, P. Gates, M. Watsky, Low access resistance perforated patch recordings using amphotericin B, J. Neurosci. Methods 37 (1991) 15–26.
[26] D.K. Lieu, J. Liu, C.W. Siu, G.P. McNerney, H.F. Tse, A. Abu-Khalil, T. Huser, R.A. Li, Absence of transverse tubules contributes to non-uniform Ca(2+) wavefronts in mouse and human embryonic stem cell-derived cardiomyocytes, Stem Cells Dev. 18 (2009) 1493–1500.
[27] J. Satin, I. Itzhaki, S. Rapoport, E.A. Schroder, L. Izu, G. Arbel, R. Beyar, C.W. Balke, J. Schiller, L. Gepstein, Calcium handling in human embryonic stem cell-derived cardiomyocytes, Stem Cells 26 (2008) 1961–1972.
[28] H. Satoh, L.M. Delbridge, L.A. Blatter, D.M. Bers, Surface:volume relationship in cardiac myocytes studied with confocal microscopy and membrane capacitance measurements: species-dependence and developmental effects, Biophys. J. 70 (1996) 1494–1504.
[29] L. Cleemann, M. Morad, Role of $Ca^{2+}$ channel in cardiac excitation-contraction coupling in the rat: evidence from $Ca^{2+}$ transients and contraction, J. Physiol. 432 (1991) 283–312.
[30] S. Kang, G. Cooper, S.F. Dunne, B. Dusel, C.H. Luan, D.J. Surmeier, R.B. Silverman, CaV1.3-selective L-type calcium channel antagonists as potential new therapeutics for Parkinson's disease, Nat. Commun. 3 (2012) 1146.
[31] A. Koschak, D. Reimer, I. Huber, M. Grabner, H. Glossmann, J. Engel, J. Striessnig, alpha 1D (Cav1.3) subunits can form l-type $Ca^{2+}$ channels activating at negative voltages, J. Biol. Chem. 276 (2001) 22100–22106.
[32] E. Carbone, H.D. Lux, Kinetics and selectivity of a low-voltage-activated calcium current in chick and rat sensory neurones, J. Physiol. 386 (1987) 547–570.
[33] B. Nilius, P. Hess, J.B. Lansman, R.W. Tsien, A novel type of cardiac calcium channel in ventricular cells, Nature 316 (1985) 443–446.
[34] J.T. Hulme, R.E. Westenbroek, T. Scheuer, W.A. Catterall, Phosphorylation of serine 1928 in the distal C-terminal domain of cardiac CaV1.2 channels during beta1-adrenergic regulation, Proc. Natl. Acad. Sci. U. S. A. 103 (2006) 16574–16579.
[35] H. Haase, S. Bartel, P. Karczewski, I. Morano, E.G. Krause, In-vivo phosphorylation of the cardiac L-type calcium channel beta-subunit in response to catecholamines, Mol. Cell. Biochem. 163–164 (1996) 99–106.
[36] L.C. Hool, Hypoxia alters the sensitivity of the L-type Ca(2+) channel to alpha-adrenergic receptor stimulation in the presence of beta-adrenergic receptor stimulation, Circ. Res. 88 (2001) 1036–1043.
[37] J.R. Williamson, S.W. Schaffer, C. Ford, B. Safer, Contribution of tissue acidosis to ischemic injury in the perfused rat heart, Circulation 53 (1976) I3–14.
[38] A. Varro, S. Hester, J.G. Papp, Caffeine-induced decreases in the inward rectifier potassium and the inward calcium currents in rat ventricular myocytes, Br. J. Pharmacol. 109 (1993) 895–897.
[39] J.P. Gomez, D. Potreau, J.E. Branka, G. Raymond, Developmental changes in Ca2+ currents from newborn rat cardiomyocytes in primary culture, Pflugers Arch. 428 (1994) 241–249.
[40] P.A. Poole-Wilson, Acidosis and contractility of heart muscle, Ciba Found. Symp. 87 (1982) 58–76.
[41] C.H. Orchard, H.E. Cingolani, Acidosis and arrhythmias in cardiac muscle, Cardiovasc. Res. 28 (1994) 1312–1319.
[42] K. Komukai, F. Brette, C. Pascarel, C.H. Orchard, Electrophysiological response of rat ventricular myocytes to acidosis, Am. J. Physiol. Heart Circ. Physiol. 283 (2002) H412–422.
[43] G. Wolkart, A. Schrammel, C.N. Koyani, S. Scherubel, K. Zorn-Pauly, E. Malle, B. Pelzmann, M. Andra, A. Ortner, B. Mayer, Cardioprotective effects of 5-hydroxymethylfurfural mediated by inhibition of L-type Ca(2+) currents, Br. J. Pharmacol. 174 (2017) 3640–3653.
[44] P. Gonzalez-Rodriguez, D. Falcon, M.J. Castro, J. Urena, J. Lopez-Barneo, A. Castellano, Hypoxic induction of T-type Ca(2+) channels in rat cardiac myocytes: role of HIF-1alpha and RhoA/ROCK signalling, J. Physiol. 593 (2015) 4729–4745.
[45] S. Martewicz, F. Michielin, E. Serena, A. Zambon, M. Mongillo, N. Elvassore, Reversible alteration of calcium dynamics in cardiomyocytes during acute hypoxia transient in a microfluidic platform, Integr. Biol. (Camb.) 4 (2012) 153–164.
[46] W. Wei, Y. Liu, Q. Zhang, Y. Wang, X. Zhang, H. Zhang, Danshen-enhanced cardioprotective effect of cardioplegia on ischemia reperfusion injury in a human-induced pluripotent stem cell-derived cardiomyocytes model, Artif. Organs 41 (2017) 452–460.
[47] B. Prod'hom, D. Pietrobon, P. Hess, Interactions of protons with single open L-type calcium channels. Location of protonation site and dependence of proton-induced current fluctuations on concentration and species of permeant ion, J. Gen. Physiol. 94 (1989) 23–42.
[48] D.S. Krafte, R.S. Kass, Hydrogen ion modulation of Ca channel current in cardiac ventricular cells. Evidence for multiple mechanisms, J. Gen. Physiol. 91 (1988) 641–657.
[49] U. Klockner, G. Isenberg, Calcium channel current of vascular smooth muscle cells: extracellular protons modulate gating and single channel conductance, J. Gen. Physiol. 103 (1994) 665–678.
[50] D.A. Katzka, M. Morad, Properties of calcium channels in guinea-pig gastric myocytes, J. Physiol. 413 (1989) 175–197.
[51] H. Ohmori, M. Yoshii, Surface potential reflected in both gating and permeation mechanisms of sodium and calcium channels of the tunicate egg cell membrane, J. Physiol. 267 (1977) 429–463.
[52] T. Iijima, S. Ciani, S. Hagiwara, Effects of the external pH on Ca channels: experimental studies and theoretical considerations using a two-site, two-ion model, Proc. Natl. Acad. Sci. U. S. A. 83 (1986) 654–658.
[53] N. Matsuda, T. Mori, H. Nakamura, M. Shigekawa, Mechanisms of reoxygenation-induced calcium overload in cardiac myocytes: dependence on pHi, J. Surg. Res. 59 (1995) 712–718.
[54] M. Kaibara, M. Kameyama, Inhibition of the calcium channel by intracellular protons in single ventricular myocytes of the guinea-pig, J. Physiol. 403 (1988) 621–640.
[55] H. Irisawa, R. Sato, Intra- and extracellular actions of proton on the calcium current of isolated guinea pig ventricular cells, Circ. Res. 59 (1986) 348–355.
[56] U. Klockner, G. Isenberg, Intracellular pH modulates the availability of vascular L-type $Ca^{2+}$ channels, J. Gen. Physiol. 103 (1994) 647–663.
[57] G. Kanaporis, R. Treinys, R. Fischmeister, J. Jurevicius, Metabolic inhibition reduces cardiac L-type $Ca^{2+}$ channel current due to acidification caused by ATP hydrolysis, PLoS One 12 (2017) e0184246.
[58] F. Di Lisa, P.S. Blank, R. Colonna, G. Gambassi, H.S. Silverman, M.D. Stern, R.G. Hansford, Mitochondrial membrane potential in single living adult rat cardiac myocytes exposed to anoxia or metabolic inhibition, J. Physiol. 486 (Pt 1) (1995) 1–13.
[59] J.A. Scaringi, A.O. Rosa, M. Morad, L. Cleemann, A new method to detect rapid oxygen changes around cells: how quickly do calcium channels sense oxygen in cardiomyocytes? J. Appl. Physiol. 115 (2013) (1985) 1855–1861.
[60] N. Saegusa, E. Moorhouse, R.D. Vaughan-Jones, K.W. Spitzer, Influence of pH on Ca(2)(+) current and its control of electrical and Ca(2)(+) signaling in ventricular myocytes, J. Gen. Physiol. 138 (2011) 537–559.
[61] Y.W. Kwan, R.S. Kass, Interactions between $H^+$ and $Ca^{2+}$ near cardiac L-type calcium channels: evidence for independent channel-associated binding sites, Biophys. J. 65 (1993) 1188–1195.
[62] P. Zhou, Y.T. Zhao, Y.B. Guo, S.M. Xu, S.H. Bai, E.G. Lakatta, H. Cheng, X.M. Hao, S.Q. Wang, Beta-adrenergic signaling accelerates and synchronizes cardiac ryanodine receptor response to a single L-type $Ca^{2+}$ channel, Proc. Natl. Acad. Sci. U. S. A. 106 (2009) 18028–18033.
[63] R. Zhu, M.A. Millrod, E.T. Zambidis, L. Tung, Variability of action potentials within and among cardiac cell clusters derived from human embryonic stem cells, Sci. Rep. 6 (2016) 18544.
[64] M. Warren, K.W. Spitzer, B.W. Steadman, T.D. Rees, P. Venable, T. Taylor, J. Shibayama, P. Yan, J.P. Wuskell, L.M. Loew, A.V. Zaitsev, High-precision recording of the action potential in isolated cardiomyocytes using the near-infrared fluorescent dye di-4-ANBDQBS, Am. J. Physiol. Heart Circ. Physiol. 299 (2010) H1271–1281.
[65] K.L. Perkins, Cell-attached voltage-clamp and current-clamp recording and stimulation techniques in brain slices, J. Neurosci. Methods 154 (2006) 1–18.
[66] B. Sakmann, E. Neher, Patch clamp techniques for studying ionic channels in excitable membranes, Annu. Rev. Physiol. 46 (1984) 455–472.
[67] E. Neher, B. Sakmann, The patch clamp technique, Sci. Am. 266 (1992) 44–51.
[68] M. Vornanen, Excitation-contraction coupling of the developing rat heart, Mol. Cell. Biochem. 163–164 (1996) 5–11.
[69] M. Vornanen, Contribution of sarcolemmal calcium current to total cellular calcium in postnatally developing rat heart, Cardiovasc. Res. 32 (1996) 400–410.
[70] R.M. Snopko, A.S. Aromolaran, K.L. Karko, J. Ramos-Franco, L.A. Blatter, R. Mejia-Alvarez, Cell culture modifies $Ca^{2+}$ signaling during excitation-contraction coupling in neonate cardiac myocytes, Cell Calcium 41 (2007) 13–25.
[71] A.P. Ziman, N.L. Gomez-Viquez, R.J. Bloch, W.J. Lederer, Excitation-contraction coupling changes during postnatal cardiac development, J. Mol. Cell. Cardiol. 48 (2010) 379–386.